

MORE WIDESPREAD THAN SUPPOSED: PRESERVED LAWSONITE IN THE BLUESCHIST-FACIES OPHIOLITIC BODIES FROM THE ALBERGIAN UNIT (LIGURIA-PIEMONTE ZONE, WESTERN ALPS)

Alberto Corno*✉, Pietro Mosca**, Chiara Groppo*, Alessandro Borghi* and Marco Gattiglio*

* Department of Earth Sciences, University of Torino, Italy

** IGG-CNR, Turin, Italy

✉ Corresponding author, e-mail: alberto.corno@unito.it

Keywords: lawsonite; thermodynamic modeling; tectono-metamorphic evolution; Albergian Unit; Liguria-Piemonte zone; Western Alps.

ABSTRACT

The Albergian unit (AU), belonging to the Liguria-Piemonte oceanic domain of the Western Alps, comprises a thick sequence of calcschists and minor meta-ophiolitic bodies, from metric to kilometric in size. The occurrence of fresh lawsonite in its metasedimentary cover is known since the end of the XIX century. This paper reports the occurrence of fresh lawsonite also in the metamafic rocks and presents petrological data to constrain the tectono-metamorphic evolution of one of these metamafic bodies exposed in the upper Chisone Valley. In the Monte Albergian - Gran Mioul area, the AU consists of a kilometric body of basalt and/or diabase metabreccias (with minor metagabbros and meta-plagiogranite clasts and blocks), covered by discontinuous layers of quartzitic metasandstones, black micaschists, and eventually a thick sequence of calcschists. This paper focuses on the petrographic and mineral chemistry features of these lithologies, with emphasis on the preserved magmatic textures in the metamafic clasts, and on fresh lawsonite occurrence and its replacement. The second part of the paper deals with phase equilibrium modeling of two representative samples from the area: a Mg-Al metagabbro and a metabreccia with plagiogranite clasts. Thermodynamic modeling of isochemical phase diagrams (i.e., P-T pseudosections), performed for the first time in this unit, allowed constraining the metamorphic peak in the lawsonite blueschist-facies conditions, at about 18-21 kbar and 380-430°C, followed by a partial re-equilibration in the epidote-stability field.

INTRODUCTION

Lawsonite-bearing metamorphic rocks, characteristics of eclogite- and blueschist-facies conditions, have been documented in many orogenic belts and are regarded as major markers of exhumed fossil subduction zones (e.g., Tsujimori and Ernst, 2014; Whitney et al., 2020). Lawsonite is a hydrous mineral retaining up to 12 wt% of H₂O; due to its stability up to depths of 300 km, it is one of the major H₂O carriers in cold subduction zones (Faccenda, 2014; Schmidt and Poli, 1994; Poli and Schmidt, 1998; van Keken et al., 2011). Moreover, the stability field of lawsonite-bearing assemblages in mafic rocks is strongly influenced by fluid composition, especially its X(CO₂) [i.e., CO₂/(H₂O+CO₂)] (Goto et al., 2007; Poli et al., 2009), making lawsonite a key mineral in order to understand carbonation/decarbonation processes in subduction zones. Thus, lawsonite should be considered a crucial mineral both for defining metamorphic conditions and for understanding fluid-rock interaction processes during the evolution of orogenic belts. However, lawsonite is a mineral prone to be easily retrogressed during both prograde and retrograde metamorphism and it has been reported as a preserved mineral only in few eclogite- and blueschist-facies orogens worldwide (Whitney et al., 2020, for a review). Recognizing prograde and/or retrograde lawsonite is, therefore, crucial to correctly define burial/exhumation processes, (paleo)geothermal gradients, and geochemical processes in tectonic reconstructions of collisional orogen.


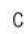


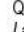


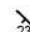

In the exhumed accretionary wedge of the Western Alps (Fig. 1a), lawsonite-bearing rocks have been documented in the Liguria-Piemonte oceanic units and in the continental units of the Sesia-Lanzo zone since the late 19th century (among the numerous papers, e.g., Franchi 1895; 1897; Ellenberger, 1960; Compagnoni, 1977; Pognante et al., 1980;

1991; Mevel and Kienast, 1980; Martin and Tartarotti, 1989; Desmons, 1990; Groppo and Castelli, 2010; Zucali and Spalla, 2011; Lefeuvre et al., 2020). Focusing on the Liguria-Piemonte oceanic units (LP), preserved lawsonite relicts (and its pseudomorphs) have been reported in two eclogite-facies units: (i) the Voltri Unit (Scarsi et al., 2018 and references therein), and (ii) the Monviso Unit (Groppo and Castelli, 2010). In addition, fresh lawsonite-bearing metamafic (and metasedimentary) rocks are widespread in the eclogite- and blueschist-facies units of Alpine Corsica (Vitale Brovarone et al., 2011; 2013; 2014a). In the blueschist-facies domain of the Western Alps, fresh lawsonite has been notably observed in the metasediments (e.g., Pognante, 1991; Lefeuvre et al., 2020; Agard, 2021): the abundance of lawsonite in metasediments has been generally linked to decarbonation processes, which mobilize Ca from calcium carbonate making it available for the lawsonite growth (Nitsch, 1972; Cook-Kollars et al., 2014). However, fresh lawsonite in mafic bodies associated with these blueschist-facies metasediments is scarcely documented in the literature (Caron, 1977; Vitale Brovarone et al., 2020; Agard, 2021 and references therein).

This contribution presents new petrographic and petrological data on the ophiolite-bearing Albergian Unit (AU hereafter; Fig. 1b), a blueschist-facies unit exposed in the Western Alps. In this unit, Caron (1974; 1977) recognized two “generations” or families of lawsonite in the metasediments: *type I “fossil”* (i.e., relict) lawsonite, crossed by the main foliation and *type II* syn-kinematic lawsonite still preserved as fresh and only locally retrogressed by white mica + zoisite + chlorite.

New original studies allowed us to observe well-preserved lawsonite crystals both in the metasedimentary sequence and in the associated metamafic rocks. New P-T estimates of the Alpine metamorphic evolution of this unit have been defined applying the isochemical phase diagram approach.

Geological map of the Albergian Unit (AU) in the Monte Albergian - Gran Mioul area

-  Undifferentiated quaternary cover
-  Carbonate micaschist (calcschist, cs). Early Cretaceous?
-  Black micaschist (bm). Late Jurassic? - Early Cretaceous?
-  Quartzitic metasandstone (qz). Late Jurassic?
-  Basaltic metabreccia (Mb), a: main gabbroic clasts and blocks. Middle Jurassic?
-  Main foliation (S2)
-  Post-D2 fold axis
-  Lithostratigraphic contact
-  Fault (dashed where inferred)

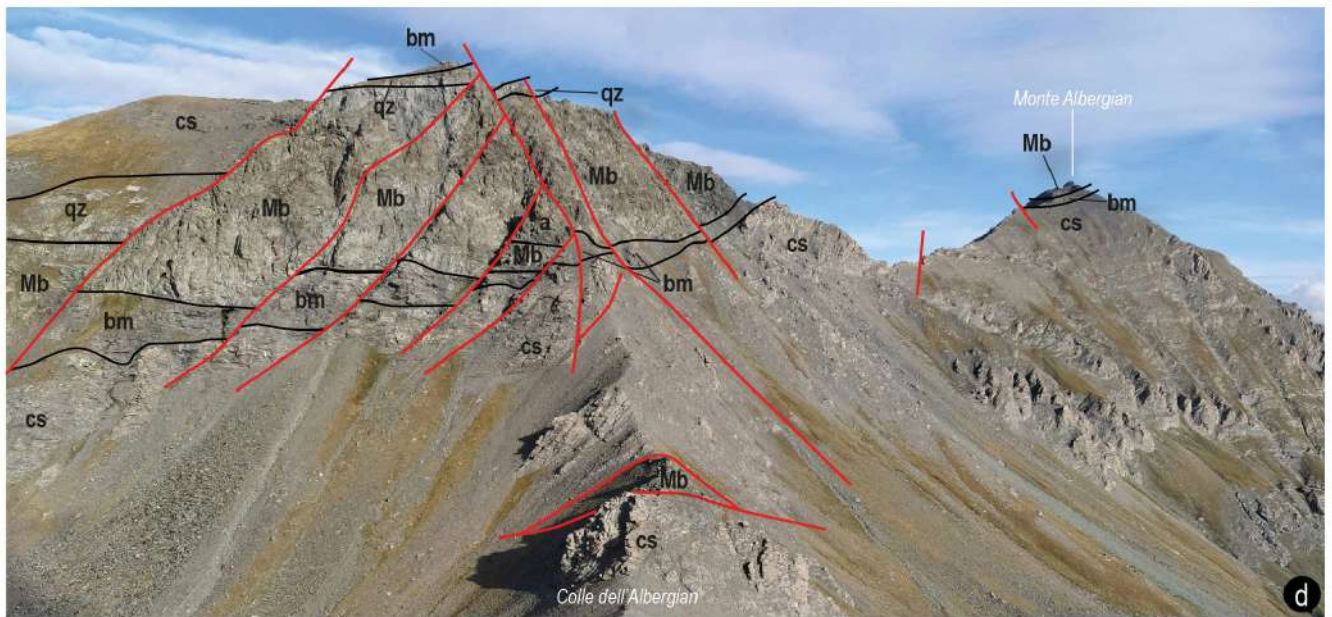
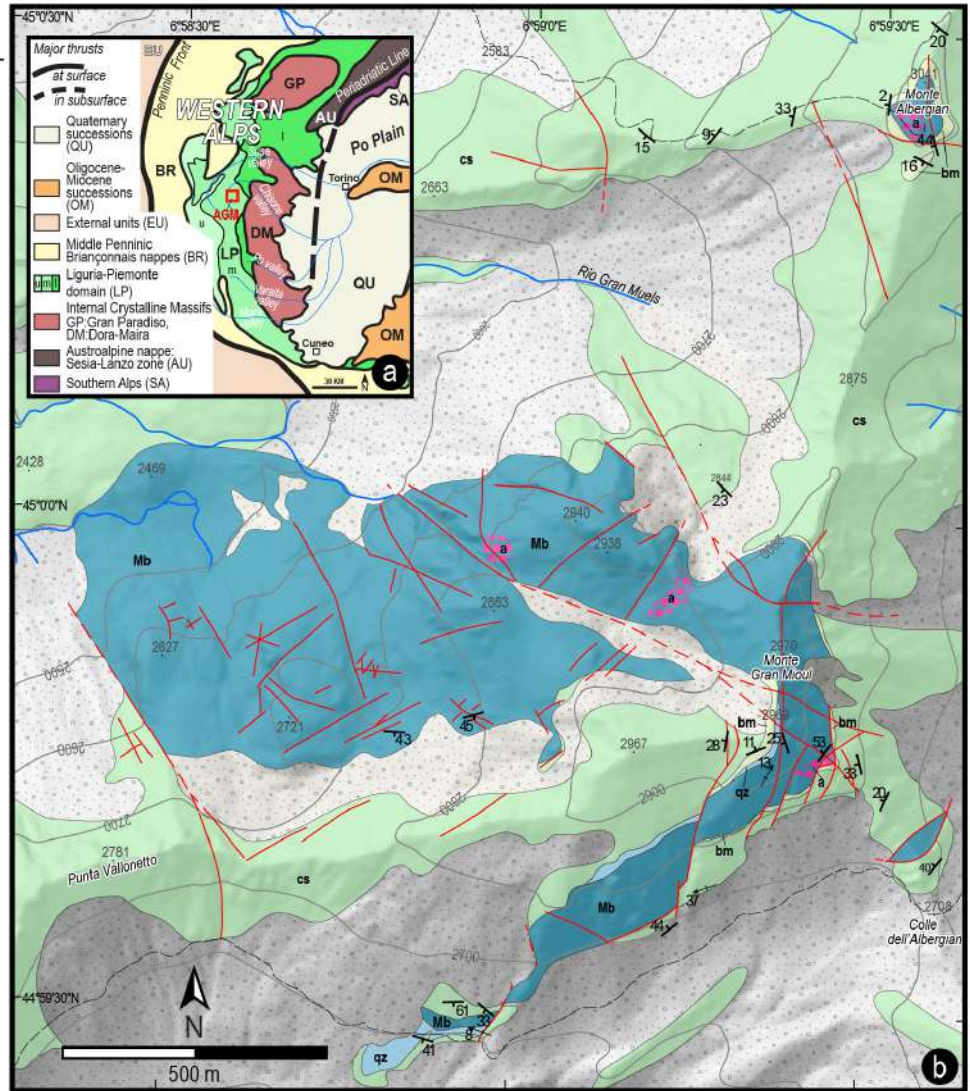
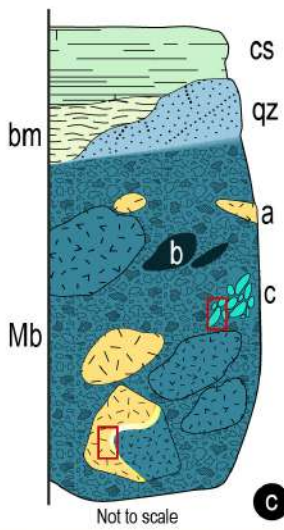


Fig. 1 - a) General and schematic map of the Western Alps. The Liguria-Piemonte oceanic domain (LP) is subdivided according to Agard (2021), u: blueschist to subgreenschist-facies units; m: epidote- and lawsonite blueschist-facies units; l: blueschist-eclogite to eclogite-facies units; b) Geological map of the Albergian - Gran Mioul area, (upper Chisone Valley, Italian Western Alps). c) schematic lithostratigraphic log of the mafic body of the Albergian - Gran Mioul area within the AU. Abbreviations are according to map legend. Blocks with different internal patterns in Mb refer to metric or plurimetric clasts and blocks of different lithologies; a: Mg-Al metagabbro; b: Fe-Ti metagabbro; c: metaplagiogranite. Red squares show the location of samples used for thermodynamic modeling; d) view on the southern side of Monte Gran Mioul. Acronyms and color lines are according to the legend of the geological map. Note the high frequency of faults and major fractures in the metamafic rocks and the “klippe-like” structure capping the summit of Monte Albergian (photo courtesy of M. Giovo).

GEOLOGICAL SETTING

The metamorphic Liguria-Piemonte oceanic units (LP) exhumed in the Western Alps sampled different segments of the oceanic domain opened in Jurassic time between the Eurasian and Adriatic plates, and can also include part of the ocean-continent transition zones (Beltrando et al., 2010; Corno et al., 2019). The LP units recorded eclogite-facies or blueschist-facies Alpine metamorphic peaks, followed by a widespread exhumation-related greenschist overprint (Beltrando et al. 2010 and references therein).

The tectonic pile exposed in the upper Susa and Chisone valleys include west-dipping LP units consisting of abundant carbonatic metasediments (Jurassic to Cretaceous in age), with variable amounts of continental and/or oceanic detrital intercalations, and bodies and (mega)blocks of mafic-ultramafic rocks locally preserving their Jurassic radiolarian and meta-limestone covers (e.g., Serv. Geol. d'It., 2002a; 2002b; 2020; Piana et al., 2017 and references therein).

A threefold subdivision of LP can be recognized in this tectonic pile, based on structural setting and metamorphic conditions (constrained with Si-in-Phe barometer and the RSCM thermometer, see Agard et al., 2001, and Beyssac et al., 2002): (1) At the highest structural levels, below the ophiolitic Chenaillet and the continental margin Chaberton-Grand Hoche-Grand Argentier units (Polino et al., 1983; Agard et al., 2001), the Lago Nero unit (Polino and Lemoine, 1984; Polino et al., 2002; Burrioni et al., 2003) preserves lawsonite- and/or Mg-carpholite-bearing assemblages equilibrated at blueschist-facies conditions from 11 kbar, 330°C to 14 kbar, 350°C (Agard et al., 2001; Beyssac et al., 2002); (2) At middle structural levels, two units are recognized: the Albergian Unit and the Cerogne-Ciantiplagna Unit (Serv. Geol. d'It., 2002a; 2002b; 2020). The Albergian unit preserves lawsonite-bearing assemblages, while the Cerogne-Ciantiplagna Unit lacks fresh lawsonite and is mostly equilibrated in the epidote-stability field. P-T estimates for these units range between 15-20 kbar and 370-450°C (Agard et al., 2001; Beyssac et al., 2002). (3) The lower structural levels expose metasediments and large meta-ophiolite bodies of the Orsiera-Rocciavré Unit, which experienced a metamorphic peak at eclogite-facies conditions or at the blueschist-eclogite-facies transition (20-29 kbar, 470-550°C; Agard et al., 2001; Beyssac et al., 2002; Ghignone et al., 2020).

THE SAMPLING SITE IN THE ALBERGIAN-GRAN MIOUL AREA

Lawsonite-bearing rocks discussed in this paper were collected in the Albergian Unit along the Albergian-Gran Mioul mountain ridge (SE of the Prigelato village, upper Chisone Valley; Fig. 1a-b), culminating on the top of Monte Albergian (3041 m a.s.l.). This section is mainly characterized by calcschists embedding a km-scale body of metamafic rocks. The metamafic body mostly consists of a clast-supported basaltic metabreccia exposed with a thickness of about 200-300 m (Fig. 1c-d). This is mainly a monomictic breccia, dominated by basalt/diabase clasts (Fig. 2a) and blocks, with minor doleritic clasts (Fig. 2b). The clasts range from few centimeters to several meters in size and are hosted within a fine-grained mafic matrix. Clasts and blocks of coarse-grained, isotropic Mg-Al metagabbro, up to several meters in size, occur close to the top of Monte

Albergian. Some of these blocks display the primary contact between the diabase/basalt and the gabbro, characterized by transitional and fading edges. The magmatic coarse-grained ophitic texture of the gabbroic protolith is well preserved, with the original sites of the magmatic pyroxene and plagioclase still perfectly recognizable (Fig. 2c). Locally, minor bodies of Fe-Ti metagabbro and metadolerite occur. In addition, rare plagiogranitic clasts have been found, wrapped by the same basaltic matrix.

The whole metamafic body is covered by: (i) discontinuous levels of quartzitic metasandstones (Fig. 2d), usually a few meters thick, and (ii) discontinuous levels of black micaschists locally intercalated with impure marble layers. These are followed by a thick sequence of calcschists, containing levels and lenses of impure marbles, about ten cm thick, in the lowermost part. Clasts of impure marbles, up to pluri-cm in size, can be found in the upper part of the calcschists.

METHODS

A Scanning Electron Microscope (JEOL JSM-IT300LV) equipped with an energy-dispersive X-ray spectrometer (EDX), with an SDD (a silicon drift detector from Oxford Instruments), hosted at the Dipartimento di Scienze della Terra of the Università degli Studi di Torino, was used for the determination of major elements. The experimental conditions include: accelerating voltage 15 kV, counting time 50 s, process time 5 μ s, and a working distance of 10 mm. The measurements were conducted in high vacuum conditions. This technique, with adequate counting statistics ($> 10^6$ cnts), allows to reach sensitivity of the order of 0.05wt% and accuracy around 1%. The EDX acquired spectra were corrected and calibrated both in energy and in intensity by conducting measurements on a cobalt standard introduced in the vacuum chamber with the samples. The Microanalysis Suite Oxford INCA Energy 300, which enables spectra visualization and element recognition, was employed. A ZAF data reduction program was used for spectra quantification. The resulting full quantitative analyses were performed, using natural oxides and silicates from Astimex Scientific Limited, as standards. All the analyses were recalculated using the MINSORT computer software (Petraakis and Dietrich, 1985). Structural formulae have been calculated on the basis of 6 oxygens for pyroxene, 12 oxygens for garnet, 14 oxygens for chlorite, 11 oxygens for white mica, 8 oxygens for lawsonite and albite, 25 oxygens for epidote and 23 oxygens for amphibole. Potassic white micas have been classified as muscovite or phengite according to their Al_{tot}/Si ratio (i.e., muscovite: $Al_{tot} > 5.00$, $Si < 3.30$; phengite: $Al_{tot} < 5.00$, $Si > 3.30$). X_{Mg} of amphiboles is defined as $Mg/(Mg + Fe^{2+})$. X_{Zr} in epidote-group minerals is defined as $Al/(Al + Fe^{3+})$. Representative analyses of mineral composition are reported in Tables 1 and 2. Mineral abbreviations are according to Whitney and Evans (2010) (Wm = potassic white mica).

High-resolution multispectral maps of the thin sections used for deriving the effective bulk compositions of the investigated samples were obtained using the same SEM-EDS instrument. Operative conditions used for mapping the entire thin sections were: 15 kV accelerating voltage, 5 nA probe current, 1 μ s EDS process time, 105 cnts/s, 2.5 μ m point step, 1 msec dwell time. The raw data were processed using the MultiSpec© software to obtain the modal compositions.

Table 1 - Representative analyses from the Mg-Al meta-gabbro sample used for thermodynamic modeling.

Sample 5482 - Micro meta-gabbro																									
Mineral type	Cpx	Cpx	Cpx	Cpx	Cpx	Cpx	Cpx	Cpx	Cpx	Lws	Lws	Lws	Lws	Lws	Lws	Grt	Grt	Grt	Grt	Grt	Wm	Wm	Wm	Wm	Wm
Analysis	1	2	3	4	5	6	7	8	1	2	3	4	1	2	3	4	5	6	7	1	2	3	4	5	
SiO ₂	49.81	53.30	52.59	54.10	54.28	56.24	55.54	55.53	40.44	38.49	37.54	38.27	SiO ₂	37.62	36.78	38.46	38.09	38.14	35.90	38.24	53.29	53.65	52.90	53.05	53.83
TiO ₂	6.04	0.53	0.52	0.46	0.53	bdl	bdl	bdl	bdl	bdl	bdl	bdl	TiO ₂	bdl	bdl	bdl	bdl	bdl	bdl	bdl	bdl	bdl	bdl	bdl	bdl
Al ₂ O ₃	4.15	4.62	4.83	5.09	4.50	6.91	6.35	5.40	32.35	31.13	30.45	30.84	Al ₂ O ₃	20.71	20.50	21.16	20.92	21.03	19.66	20.99	22.91	23.46	22.56	21.30	22.20
FeO	10.15	13.38	14.87	11.96	14.45	7.70	8.30	8.54	0.65	0.67	0.82	0.60	FeO	22.98	13.82	18.08	18.70	16.29	25.02	19.16	2.67	2.39	2.95	4.06	3.19
MnO	0.26	0.33	0.36	0.32	0.45	bdl	0.36	0.24	---	---	---	---	MnO	7.07	16.37	9.84	10.12	12.62	7.90	9.11	bdl	bdl	bdl	bdl	bdl
MgO	12.95	14.65	14.55	15.96	13.76	10.00	8.70	9.93	---	---	---	---	MgO	0.62	0.45	0.53	0.69	0.51	0.49	0.53	4.76	5.25	4.75	4.53	4.61
CaO	13.00	11.77	10.89	10.73	10.37	12.66	14.95	14.62	16.05	18.80	20.07	17.87	CaO	10.06	10.94	11.88	11.53	11.59	11.10	12.23	bdl	bdl	bdl	bdl	bdl
Na ₂ O	1.80	1.42	1.65	1.92	1.86	6.98	6.02	5.99	---	---	---	---	Na ₂ O	bdl	bdl	bdl	bdl	bdl	bdl	bdl	bdl	bdl	bdl	bdl	bdl
K ₂ O	bdl	bdl	bdl	bdl	bdl	bdl	bdl	bdl	0.09	bdl	bdl	0.42	K ₂ O	bdl	bdl	bdl	bdl	bdl	bdl	bdl	10.34	9.25	10.27	11.52	10.60
Total	98.16	100.01	100.27	100.54	100.20	100.48	100.22	100.26	89.58	89.08	88.88	87.58	Total	99.07	98.86	99.95	100.05	100.17	100.08	100.27	93.97	93.99	93.43	94.45	94.43
Si	1.871	1.964	1.945	1.964	1.996	1.994	2.002	1.995	2.076	2.017	1.988	2.028	Si	3.031	2.982	3.049	3.028	3.029	2.908	3.030	3.596	3.588	3.597	3.620	3.628
Al ^{IV}	0.129	0.036	0.055	0.036	0.004	0.006	---	0.005	1.957	1.922	1.900	1.926	Al ^{IV}	---	0.018	---	---	---	0.092	---	0.809	0.824	0.807	0.761	0.744
Al ^{VI}	0.054	0.164	0.156	0.182	0.191	0.282	0.270	0.224	---	---	---	---	Al ^{VI}	1.967	1.942	1.977	1.960	1.056	1.785	1.960	2.836	2.873	2.809	2.663	2.784
Ti	0.171	0.015	0.015	0.012	0.015	---	---	---	---	---	---	---	Fe ³⁺	0.027	0.063	0.012	0.034	0.025	0.220	0.033	---	---	---	---	---
Fe ³⁺	---	---	---	---	---	0.204	0.146	0.199	---	---	---	---	Fe ²⁺	1.522	0.874	1.186	1.209	1.056	1.475	1.237	0.302	0.268	0.336	0.464	0.359
Fe ²⁺	0.235	0.276	0.300	0.237	0.291	0.023	0.104	0.056	0.028	0.029	0.036	0.026	Mn	0.483	1.124	0.660	0.681	0.849	0.542	0.612	---	---	---	---	---
Mn	0.006	0.007	0.007	0.006	0.009	---	0.011	0.007	---	---	---	---	Mg	0.075	0.054	0.062	0.081	0.061	0.059	0.062	0.959	1.047	0.963	0.920	0.926
Mg	0.534	0.538	0.523	0.563	0.494	0.491	0.467	0.514	---	---	---	---	Ca	0.868	0.950	1.010	0.983	0.986	0.963	1.038	---	---	---	---	---
Fe ²⁺	0.084	0.136	0.160	0.126	0.153	0.002	---	0.002	---	---	---	---	K	---	---	---	---	---	---	---	1.780	1.578	1.781	2.006	1.822
Mn	0.002	0.003	0.004	0.003	0.005	---	---	---	---	---	---	---	Mg	0.516	0.291	0.406	0.409	0.358	0.485	0.419	---	---	---	---	---
Mg	0.191	0.266	0.280	0.300	0.260	0.038	0.001	0.018	---	---	---	---	alm	0.164	0.374	0.226	0.230	0.287	0.178	0.207	---	---	---	---	---
Ca	0.523	0.465	0.432	0.417	0.408	0.481	0.578	0.563	0.883	1.055	1.138	1.014	sps	0.025	0.018	0.021	0.027	0.021	0.019	0.021	---	---	---	---	
Na	0.131	0.102	0.118	0.135	0.132	0.480	0.421	0.417	---	---	---	---	pyr	0.281	0.285	0.340	0.316	0.321	0.208	0.335	---	---	---	---	---
K	---	---	---	---	---	---	---	---	0.006	bdl	bdl	0.029	grs	0.013	0.031	0.006	0.017	0.013	0.109	0.017	---	---	---	---	
X _{Mg}	0.689	0.656	0.630	0.698	0.622	0.956	0.803	0.891	---	---	---	---	anr	0.013	0.031	0.006	0.017	0.013	0.109	0.017	---	---	---	---	---
X _{Na}	0.200	0.180	0.215	0.245	0.244	0.499	0.421	0.426	---	---	---	---													

Cpx: clinopyroxene; Lws: lawsonite; Grt: garnet; Wm: white mica.

Table 2 - Representative analyses from the plagiogranite meta-breccia sample used for thermodynamic modeling.

Mineral type	NaCpx	NaCpx	NaCpx	NaCpx	NaCpx	NaCpx	NaCpx	NaCpx	NaCpx	NaCpx	Lws	Lws	Lws	Lws	Lws	Lws	Lws	Lws	Lws	Lws	Wm	Wm	Wm	Wm	Wm	Wm								
Analysis	1	2	3	4	5	6	1	2	3	4	5	6	1	2	3	4	5	6	1	2	3	4	5	6	1	2	3	4	5	6				
SiO₂	57.43	56.93	54.40	58.67	56.15	57.22	57.93	57.55	57.26	58.38	58.02	58.90	SiO₂	38.09	37.99	39.04	39.61	38.22	40.82	40.82	54.51	49.67	52.51	50.98	52.27	52.74								
TiO₂	bdl	0.61	bdl	bdl	bdl	bdl	bdl	bdl	bdl	bdl	bdl	bdl	TiO₂	bdl	0.48	bdl	bdl	0.68	bdl	bdl	bdl	bdl	bdl	bdl	bdl	2.38	0.96							
Al₂O₃	9.34	12.91	10.60	16.47	5.63	9.57	4.32	5.13	3.75	6.68	6.08	7.20	Al₂O₃	30.77	29.92	31.47	31.58	29.32	31.51	21.13	25.97	22.39	24.10	20.60	19.69									
FeO*	17.67	13.69	15.29	10.47	20.79	17.87	19.43	17.38	19.56	16.35	17.32	15.67	Cr₂O₃	bdl	bdl	bdl	bdl	bdl	bdl	bdl	bdl	bdl	bdl	bdl	bdl	0.43	0.39	0.51						
MnO	bdl	bdl	bdl	bdl	bdl	bdl	bdl	bdl	bdl	bdl	bdl	bdl	FeO	0.85	1.48	0.85	1.54	2.83	1.28	3.74	5.49	4.00	5.01	4.09	4.53									
MgO	1.36	0.76	0.85	0.65	1.98	1.26	9.22	9.34	9.60	9.43	9.15	9.60	MgO	bdl	bdl	bdl	bdl	bdl	bdl	bdl	4.88	2.71	4.11	3.30	4.12	4.48								
CaO	2.01	1.58	1.40	0.82	3.39	1.95	0.28	0.35	0.41	0.21	0.24	0.00	CaO	16.50	16.47	16.94	17.36	16.61	17.17	bdl	bdl	bdl	bdl	bdl	1.93	0.42								
Na₂O	14.17	14.75	13.77	15.07	13.01	13.97	7.87	7.59	7.66	7.89	7.74	7.96	Na₂O	bdl	bdl	bdl	bdl	bdl	bdl	bdl	9.86	9.44	9.55	9.58	8.91	9.35								
K₂O	bdl	bdl	bdl	bdl	bdl	bdl	bdl	bdl	bdl	bdl	bdl	bdl	K₂O	bdl	bdl	bdl	bdl	bdl	bdl	bdl	bdl	0.29	bdl	bdl	bdl	bdl	bdl							
Total	101.98	101.23	96.30	102.15	100.94	101.85	99.06	97.34	98.24	98.95	98.55	99.33	Total	86.21	86.34	88.30	90.08	87.65	90.77	94.12	93.58	92.56	93.39	94.68	92.67									
Si	2.000	1.972	1.994	1.990	2.006	1.999	8.097	8.127	8.061	8.075	8.083	8.077	Si	2.045	2.047	2.047	2.045	2.046	2.083	3.677	3.411	3.606	3.499	3.543	3.644									
Al^{IV}	---	0.028	0.006	0.010	---	0.001	---	---	---	---	---	---	Al^{IV}	1.948	1.900	1.945	1.922	1.850	1.895	0.646	1.178	0.788	1.003	0.915	0.713									
Al^{VI}	0.383	0.499	0.452	0.649	0.237	0.393	0.712	0.854	0.622	1.088	0.999	1.164	Al^{VI}	---	---	---	---	---	---	---	2.714	3.025	2.837	2.895	2.376	2.494								
Ti	---	0.016	---	---	---	---	---	---	---	---	---	---	Ti	---	0.019	---	---	0.027	---	---	---	---	---	---	0.242	0.099								
Fe³⁺	0.574	0.488	0.533	0.352	0.653	0.554	0.877	0.708	1.039	0.584	0.671	0.564	Cr	---	---	---	---	---	---	---	---	---	---	0.047	0.041	0.056								
Fe²⁺	---	---	---	-0.055	---	---	1.394	1.344	1.263	1.307	1.346	1.232	Fe	0.038	0.067	0.037	0.066	0.127	0.054	0.422	0.631	0.460	0.576	0.463	0.524									
Mn	---	---	---	---	---	---	---	---	---	---	---	---	Mg	---	---	---	---	---	---	---	0.981	0.555	0.842	0.674	0.833	0.923								
Mg	0.071	0.039	0.047	0.033	0.105	0.066	1.920	1.966	2.014	1.945	1.900	1.962	Ca	0.950	0.951	0.952	0.961	0.952	0.938	---	---	---	---	0.280	0.062									
Fe²⁺	---	---	---	---	---	---	---	---	---	---	---	---	Na	---	---	---	---	---	---	---	---	0.077	---	---	---									
Mn	---	---	---	---	---	---	---	---	---	---	---	---	K	---	---	---	---	---	---	---	1.697	1.655	1.673	1.677	1.540	1.648								
Mg	---	---	---	---	---	---	---	---	---	---	---	---																						
Ca	0.075	0.059	0.055	0.030	0.130	0.073	0.042	0.052	0.062	0.031	0.036	bdl																						
Na	0.957	0.991	0.978	0.991	0.901	0.946	1.958	1.948	1.938	1.969	1.964	2.000																						
Na	---	---	---	---	---	---	0.176	0.131	0.154	0.147	0.127	0.117																						
K	---	---	---	---	---	---	---	---	---	---	---	---																						
X_{Mg}	---	---	---	---	---	---	0.579	0.594	0.615	0.598	0.585	0.614																						
X_{Na}	0.927	0.944	0.947	0.970	0.874	0.928	---	---	---	---	---	---																						

NaCpx: Na-clinopyroxene; Amp: amphibole; Lws: lawsonite; Wm: white mica. In Na-clinopyroxene analyses FeO* = Fe₂O₃.

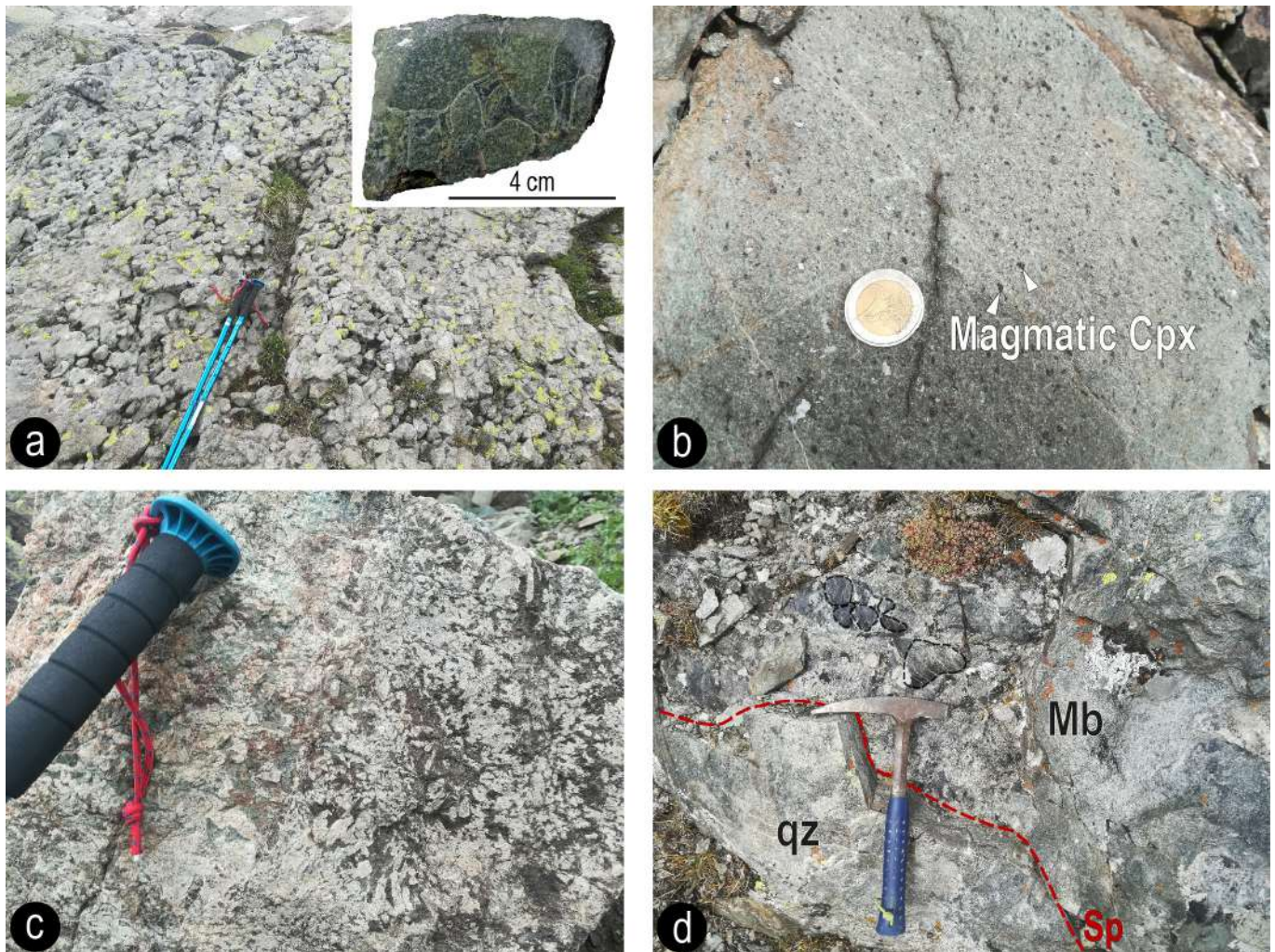


Fig. 2 - Field photographs of the Albergian - Gran Mioul area. a- differential erosion between (meta)diabase clasts, centimetric in size, and the fine-grained mafic matrix, highlighting the brecciated structure of the metamafic rocks (Monte Gran Mioul west side, 2700 m a.s.l.). The detail in the inset shows a polished sample of basaltic meta-breccia with a clast-supported texture. b- Decimetric clast of meta-dolerite consisting of mm-sized clinopyroxene crystals, weakly isoriated, within a fine-grained green matrix (Monte Gran Mioul northwest couloir, 2800 m a.s.l.). c- detail of a coarse-grained metagabbro, with magmatic ophitic texture still perfectly preserved but replaced by metamorphic minerals. Note the absence of metamorphic structures (Monte Albergian south-west face, 2990 m a.s.l.). d- lithostratigraphic contact between quartzitic metasandstone (qz), with well-developed layering (Sp main foliation) defined by alternating pluri-cm-thick quartzite layers and cm thick micaceous layers, and basaltic metabreccia (Mb). The dashed black lines highlight pluri-cm clasts within the meta-breccia (Monte Gran Mioul south face, 2600 m a.s.l.).

PETROGRAPHY AND MINERAL CHEMISTRY

More than 50 thin sections representative of all the lithologies distinguished in the studied section of AU were observed under optical microscope. In this section microstructures and petrographic features are described, with emphasis on the occurrence of lawsonite.

Three main tectono-metamorphic events have been recognized in the area: i) the older D_1 event is recorded by the oldest metamorphic foliation (S_1), defined by peak mineral assemblages, mainly preserved in the metasedimentary rocks; ii) the D_2 event is related to the development of the regional schistosity in the area (S_2), which represents the axial plane of isoclinal folds; this event is responsible for strain slip cleavage, mechanic re-orientation and recrystallization/retrogression of minerals of D_1 event; iii) the D_3 event, which is responsible for the development of open folds and for the reactivation/reorientation of older structures, occurred during greenschist-facies equilibration.

Basaltic metabreccia

Clasts and blocks of metadiabase and metabasalt consist of lawsonite \pm clinopyroxene + white mica + Na-amphibole + Ca-amphibole + quartz + epidote + chlorite + pumpellyite + albite + titanite. The fine-grained matrix is usually made of the same assemblage but lacks clinopyroxene relicts and it contains scattered calcite. Both clasts and matrix display a poorly developed S_2 foliation, defined by phengite + Na-amphibole + epidote + quartz + titanite \pm chlorite \pm pumpellyite. Magmatic Ca-clinopyroxene relicts are only locally preserved within the clasts; they are mostly retrogressed by actinolite + chlorite + albite. Lawsonite occurs both in the clasts and in the matrix (Fig. 3a) after the magmatic plagioclase, mainly preserved fresh (i.e., metastable) and locally replaced by two events of retrogression: a first one, characterized by blastesis of zoisite \pm pumpellyite, and a second one, characterized by more extensive growth of muscovite and epidote (\pm quartz) (Fig. 4a). Lawsonite is locally wrapped by patches of Na-amphibole + Ca-amphibole.

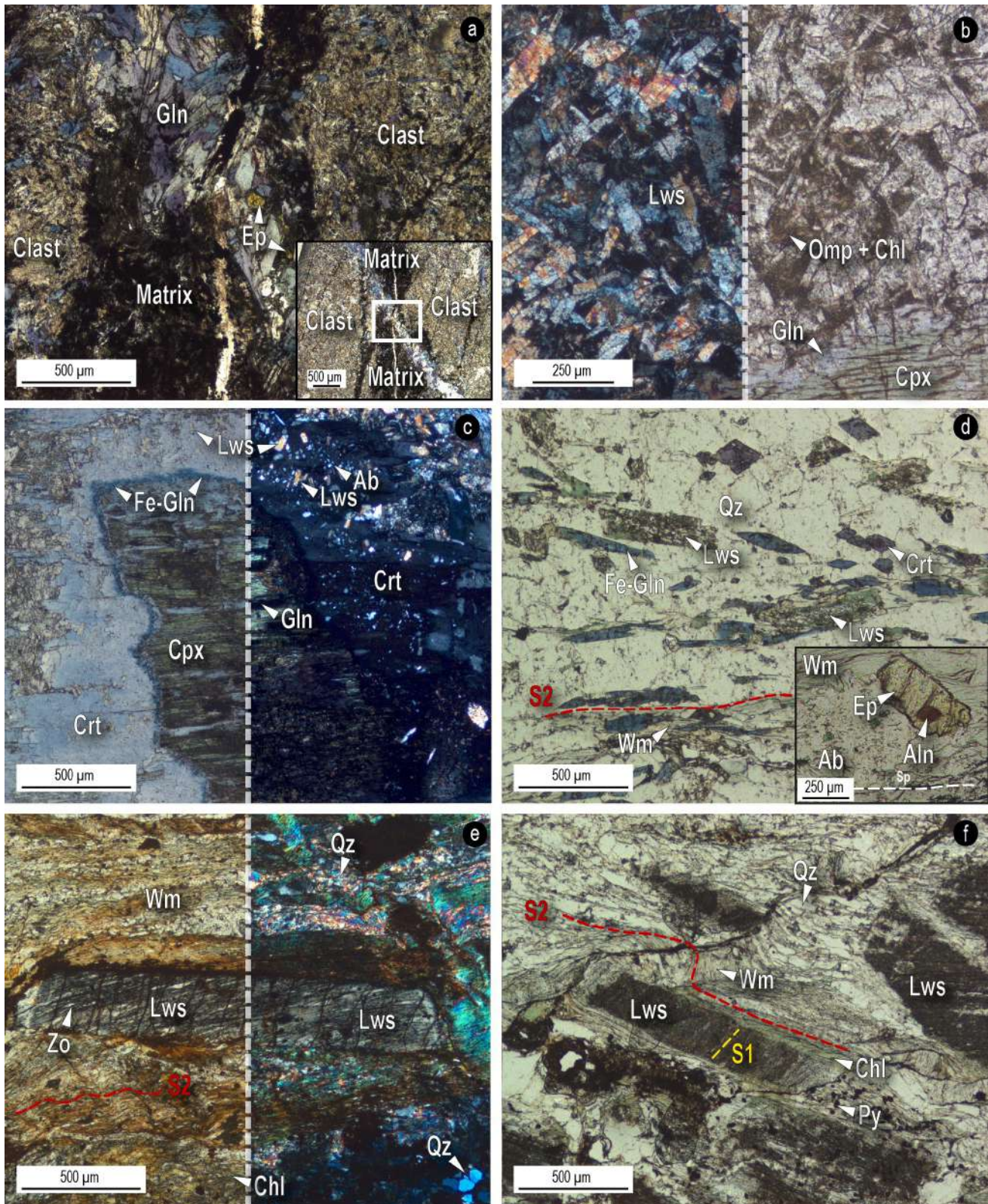


Fig. 3 - Representative microstructures and mineral assemblages under optical microscope. a- Detail of a Gln + Ep + Qz vein in a basaltic meta-breccia. The inset shows the same vein at a lower magnification: note that the vein cross-cuts both clasts and matrix (Plain Polarized Light, PPL). b- Preserved ophitic texture within a Mg-Al metagabbro consisting of idioblastic (cumulitic) magmatic plagioclase sites, now replaced by an aggregate of idioblastic lawsonite + interstitial omphacite and chlorite, and by the intercumulus clinopyroxene domains (lower right), in which the magmatic clinopyroxene is partially replaced at rims by glaucophane (left-side Crossed Polarized Light, XPL, right-side PPL). c- Fe-Ti meta-gabbro characterized by a magmatic clinopyroxene core (Cpx), partially retrogressed by Na-amphibole. In detail, an inner coronitic texture of glaucophane grows on clinopyroxene core and it is itself replaced by a thin outer mantle of Fe-glaucophane and a widespread rim of crossite. Note lawsonite crystals dispersed within the outer edge of crossite (left-side PPL, right-side XPL). d- Quartzitic metasandstone characterized by iso-oriented white mica, lawsonite, and Na-amphibole. Crossite (lavender in color) overgrows Fe-glaucophane crystals (bluish). The inset shows a detail of epidote with a detrital allanitic core (PPL). e- Black micaschist characterized by mm crystals of lawsonite, only partially retrogressed by zoisite and quartz (left-side PPL, right-side XPL). f- Calcschist characterized by cloudy lawsonite crystals wrapped by the main foliation (S_2). A relict pre- S_2 foliation is preserved in the cores of lawsonite crystals, highlighted by quartz + pyrite (PPL).

Na-amphibole crystals are locally overgrown by poikiloblastic albite, chlorite, and Ca-amphibole. Basaltic metabreccias are locally crosscut by a network of veins at variable angles with respect to the main S_2 foliation, resulting syn to post- D_2 event. These veins, filled by quartz + idiomorphic Na-amphibole + epidote, crosscut both the clasts and the matrix (Fig. 3a).

Lawsonite is characterized by a significant Ti + Cr + Fe substitution of the Al site (Fig. 5a). Three different generations of white mica have been recognized: the syn- D_1 phengite displays the highest Si content (Si up to 3.71 a.p.f.u.), the syn- D_2 phengite have Si in the range 3.35-3.50 a.p.f.u., whereas a marked decrease in Si is observed in the syn- D_3 muscovite flakes (Si < 3.30 a.p.f.u.; Fig. 5b). The relict magmatic Ca-clinopyroxenes have augitic and pigeonitic compositions (Fig. 5c). Na-amphiboles plot in the glaucophane and crossite fields, while Ca-amphiboles plot in the actinolite field (Fig. 5e-f) (Leak, 1978; Hawthorne et al., 2012). Na-amphiboles occurring in the second deformation event display shifting compositions, from glaucophane to crossite. X_{Mg} of Na-amphiboles ranges from 0.62 to 0.77, while X_{Mg} of actinolite ranges from 0.34 to 0.83. Epidote-group minerals grow as zoisite during the D_2 event and as epidote during the D_3 event (Fig. 5d).

Metagabbro bodies

Metagabbro clasts, pods, and lenses still preserve their original coarse-grained magmatic texture. They can be classified as Mg-Al metagabbros (better developing and preserving the peak assemblage) and Fe-Ti metagabbros.

Mg-Al metagabbros are made of lawsonite + Ca-clinopyroxene + omphacite + white mica + Na-amphibole + Ca-amphibole + epidote + chlorite + albite + rutile + titanite and rare quartz. Small subhedral crystals of garnet have been occasionally found only in rare fine-grained metagabbros (e.g., sample 5482). Mg-Al metagabbros are often characterized by a perfectly preserved ophitic structure, with the idiomorphic sites of magmatic plagioclase now completely replaced by aggregates of idiomorphic lawsonite, up to 500 μm in size, and the intercumulus domains originally consisting of clinopyroxene still recognizable (Fig. 3b). Lawsonite crystals include small patches of quartz, suggesting they grew in SiO_2 -saturated domains (Fig. 4b). Although generally perfectly preserved, lawsonite is locally replaced by two distinct retrograde assemblages, the first consisting of zoisite + paragonite, and the second of muscovite + epidote \pm pumpellyite. The plagioclase sites as a whole are locally replaced at rims by white mica + albite + pumpellyite aggregates. The intercumulus magmatic Ca-clinopyroxene is often still preserved; it is only locally replaced, along fractures and rims, by Na- and Ca-amphiboles (Fig. 3b) and by minor omphacite. Few veins crosscut the Mg-Al metagabbros, usually consisting of quartz and albite.

In Mg-Al metagabbros three different generations of white mica have been identified: syn- D_1 phengite (Si up to 3.67 a.p.f.u.), minor syn- D_2 phengite (Si from 3.35 to 3.45 a.p.f.u.), and syn- D_3 muscovite (Si < 3.25 a.p.f.u.; Fig. 5b), which is the most widespread white mica. Clinopyroxene composition ranges from Ca-pyroxene to Ca-Na-pyroxene (Fig. 5c). It is worth noting that the large relicts of "magmatic" clinopyroxenes already contain low amounts of Na, whose abundance increases gradually in fine-grained clinopyroxenes occurring in the matrix. "Magmatic" clinopyroxenes plot in the diopside, augite, and pigeonite fields, whilst D_1 metamorphic clinopyroxenes plot in the omphacite field

(Morimoto, 1988). A first generation of Na-amphibole plots in the glaucophane field, while a second one, related to the late stages of the D_2 event, plots in the crossite field (Fig. 5f). Both these generations of Na-amphibole are often overgrown by actinolite (Fig. 5e). X_{Mg} of Na-amphiboles ranges from 0.67 to 0.83, while for actinolite it ranges from 0.61 to 0.85. Epidote-group minerals occur as a first generation of zoisite and a second generation of epidote (Fig. 5d).

Fe-Ti metagabbros consist of Na-amphiboles + Ca-clinopyroxene relicts + Ca-Na clinopyroxene + lawsonite + white mica + epidote + albite + chlorite + titanite + rutile (Fig. 3c). The magmatic Ca-clinopyroxene is locally still preserved, but it is mostly replaced by metamorphic Ca-Na pyroxenes and by different types of Na-amphiboles + minor zoisite and chlorite. The metamorphic Ca-Na clinopyroxenes occur in two generations (Fig. 5c): earlier exsolution lamellae with acmite/aegirine-augite composition (Fig. 5d) occur at a high angle with respect to the main cleavages, whereas a later omphacite generation grew along the main cleavages within larger magmatic clinopyroxenes (Fig. 4d). At least three generations of Na-amphibole occur in different domains of the magmatic clinopyroxene sites (Fig. 5f): glaucophane is concentrated in the core, Fe-glaucophane forms a thin mantle and crossite forms a thick rim (Figs. 3c and 4c). The magmatic plagioclase domains are more difficult to be recognized, because pervasively retrogressed. Lawsonite usually occurs in patches, partially or completely retrogressed by chlorite + albite or by muscovite + epidote, or as μm relicts in Na-amphibole (Fig. 4c). White mica is usually not abundant and occurs as syn- D_3 muscovite patches with epidote, retrogressing previous lawsonite crystals (Fig. 5b).

Plagiogranites

Plagiogranite clasts consist almost exclusively of Na-pyroxene, lawsonite, and quartz with minor white mica + Na-amphibole + zoisite + albite + chlorite and titanite (Fig. 6c). The plagiogranite clasts are embedded in a matrix similar to that of basaltic metabreccia and made of Na-amphibole + white mica + epidote + quartz + chlorite + albite and minor lawsonite. A weak S_2 foliation is defined by Na-amphibole + white mica + epidote + quartz. Lawsonite is usually well preserved and only locally replaced by zoisite and quartz. White mica is often associated with titanite, suggesting it replaced magmatic biotite. Clinopyroxenes plot both in the jadeite field and in the acmite field (Morimoto, 1988; Figs. 5c and 6f) and are only seldom replaced by Na-amphiboles and chlorite. Na-amphibole compositions plot at the transition between glaucophane and crossite fields (Fig. 5f).

The S_2 foliation is cross-cut by quartz + albite and quartz + albite + Na-amphibole veins.

Quartzitic metasandstones

Quartzitic metasandstones consist of quartz + white mica + Na-amphibole + epidote + lawsonite + chlorite + albite + detrital allanite and ilmenite. The main foliation (S_2) is defined by mm-thick white mica + Na-amphibole + lawsonite discontinuous layers alternated with pluri-mm thick discontinuous quartz domains (Fig. 3d). Lawsonite is preserved as euhedral to subhedral crystals, variably overgrown by zoisite + quartz (Fig. 4e). A late retrogression rarely occurs, linked to muscovite + epidote blastesis. Na-amphibole crystals are locally replaced by poikiloblastic albite and epidote + chlorite assemblages. Allanite occurs as relict crystals overgrown by epidote (Fig. 3d).

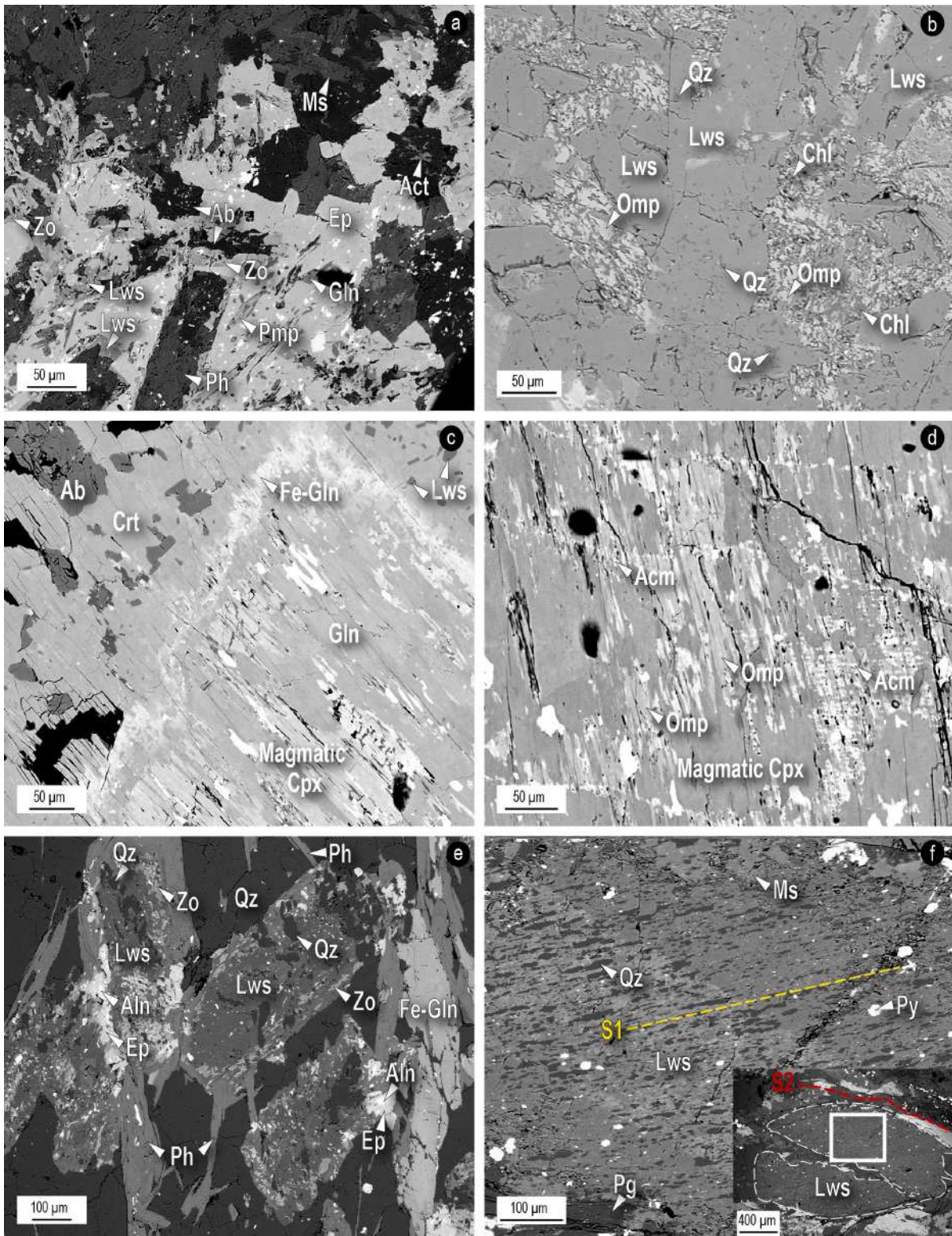


Fig. 4 - Representative microstructures and mineral assemblages under SEM (backscattered electron images, BSE). a- Lawsonite crystals almost completely replaced by phengite, zoisite, and pumpellyite in a basaltic metabreccia. Note the widespread occurrence of epidote, retrogressing both lawsonite and zoisite; b- Detail of the plagioclase domain reported in Fig. 3b. Lawsonite crystals include μm -sized “drops” of quartz; omphacite + chlorite growing in the intercumulus matrix do not display any preferential orientation. c- Clinopyroxene domain in a Fe-Ti metagabbro: the magmatic clinopyroxene, still preserved in the core, is mostly replaced by three different types of Na-amphiboles: glaucophane in the core, Fe-glaucophane in the thin mantle, and crossite in the thick rim. Crossite includes sub-idioblastic crystals of lawsonite and is partially retrogressed by albite at the rim. d- detail of a magmatic clinopyroxene domain from a Fe-Ti meta-gabbro: the magmatic Cpx is replaced by two generations of metamorphic clinopyroxene. An earlier generation of acmite (developed at a high angle with respect to the main cleavages in the crystals) is overgrown by later omphacite (light gray). e- Lawsonite crystals of a quartzitic metasandstone replaced by zoisite at rims and including quartz in the core. Epidote, often with an allanitic core, occurs both over lawsonite and Fe-glaucophane. f- Lawsonite porphyroblast from a calcschist, preserving an early pre- S_2 foliation, defined by quartz and pyrite. The core of the lawsonite is slightly enriched in Ti + Fe and it appears brighter. The main foliation S_2 (see full image in the inset) wraps around the lawsonite crystal and is defined by muscovite and paragonite, growing at rims of the lawsonite.

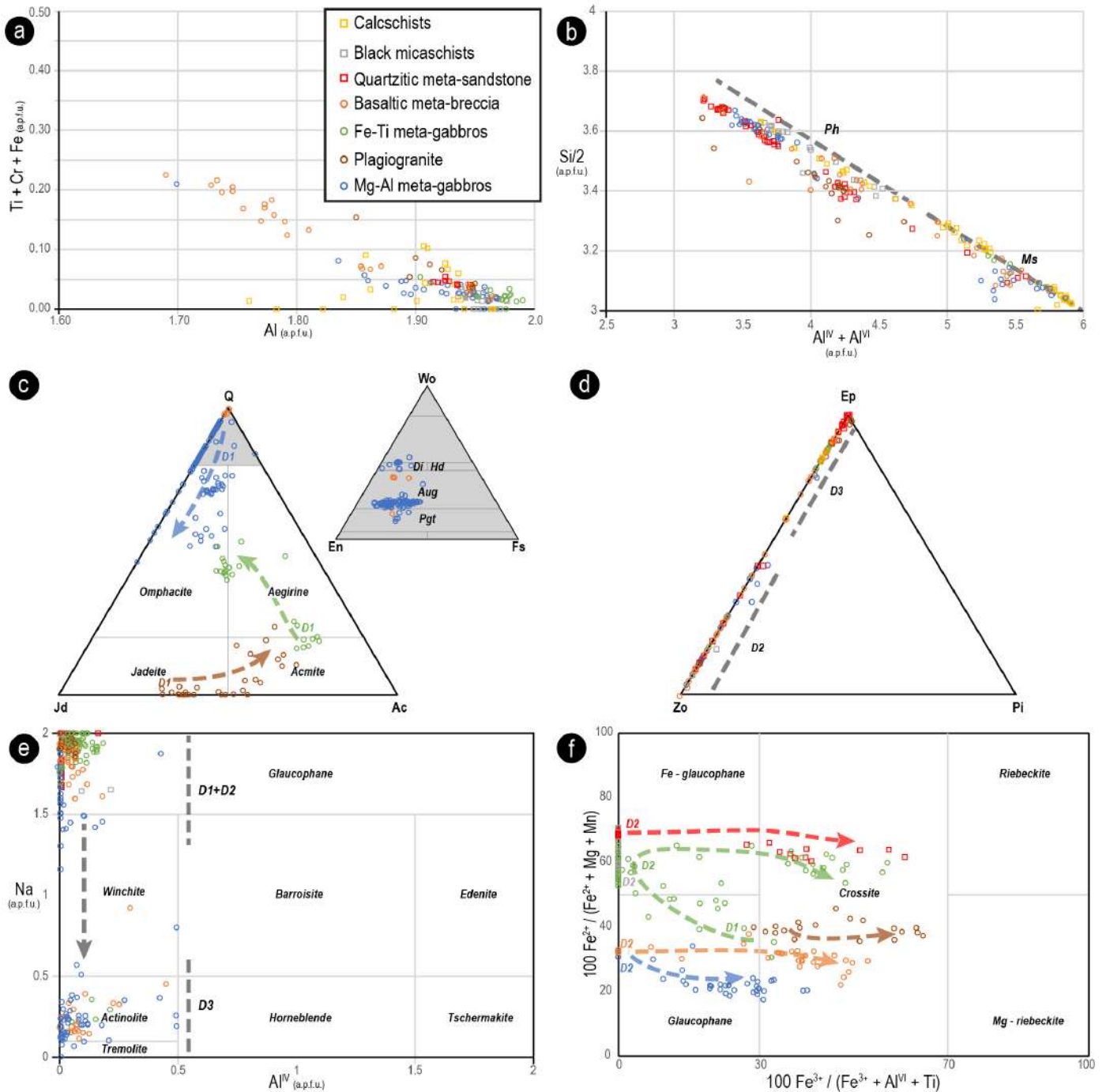


Fig. 5 - Mineral chemistry and classification diagrams. a) Lawsonite Al-site composition, showing that the transition metals (i.e. Fe + Ti + Cr) slightly substitute Al in the lawsonite structure. b) White mica composition in the Si vs ($Al^{IV} + Al^{VI}$) diagram, showing three distinct generations of white mica in most of the investigated lithologies. Muscovitic compositions are systematically related to the D_3 event; phengitic compositions are related to the D_1 and D_2 events and define two distinct clusters in most of the investigated samples (with a partial overlap for a few of them). c) Morimoto (1988) pyroxene diagram; the Q vertex for magmatic clinopyroxene is reported in grey on the right. The arrows highlight changes in compositions between different generations of clinopyroxene, as suggested by microstructural evidence; each clinopyroxene generation has been related to a specific tectono-metamorphic stage (mag: magmatic relicts; D_1 : first deformation stage). Note the gradual Na-enrichment in the clinopyroxenes from meta-gabbros and the occurrence of three different magmatic clinopyroxenes. d) Epidote-group minerals diagram highlighting the occurrence of two generations of epidote minerals: D_2 zoisite and D_3 epidote. e- Amphibole composition in the Hawthorne et al. (2012) diagram Na vs Al^{IV} . D_1 and D_2 amphiboles plot in the Glaucophane (Na-amphibole) field, while D_3 Ca-amphibole rarely enters in the tremolite field. f- Na-amphibole classification according to the $Fe^{3+}/(Fe^{3+} + Al^{VI} + Ti)$ vs. $Fe^{2+}/(Fe^{2+} + Mg + Mn)$ diagram. While amphiboles from metamafic rocks (i.e. metagabbros and metabasites) generally plot in the Mg-rich glaucophane field, amphiboles from the metasedimentary lithologies usually plot in the Fe-rich glaucophane field. A general trend towards Fe^{3+} -enriched compositions (Crossite) is generally observed through all samples and is highlighted by dashed arrows and labels (D_1 : first deformation stage; D_2 : second deformation stage). The reader is referred to the PDF of the article for a colour version.

The first generation of Na-amphibole can be classified as Fe-glaucophane, while a second generation has a crossitic composition (Fig. 5f). Three generations of white mica occur in different microstructural positions: syn-D₊ phengite flakes (Si up to 3.71 a.p.f.u.) are often found in poikiloblastic albite, syn-D₂ phengite (Si from 3.47 to 3.35 a.p.f.u.) defines the main foliation that wraps pre-kinematic crystals of lawsonite; both syn-D₁ and -D₂ flakes are partially replaced by syn-D₃ muscovite (Si < 3.27 a.p.f.u.), which only locally develops an incipient syn-D₃ micro-crenulation cleavage (Fig. 5b). Epidote-group minerals occur as zoisite, overgrowing lawsonite, and epidote, overgrowing allanite relicts (Fig. 5d).

The S₂ foliation is cross-cut by veins filled by epidote (near the contact with metamafic rocks) and by albite + quartz.

Black micaschists

Black micaschists consist of white mica + quartz + lawsonite + Na-amphibole + chlorite + epidote + albite + calcite + graphite and accessory rutile and titanite. They are characterized by a compositional banding defined by white mica + lawsonite + Na-amphibole + chlorite domains alternated with quartz ± calcite domains.

Lawsonite occurs as large, pluri-mm porphyroblasts (Fig. 3e), pre-kinematic with respect to the main S₂ foliation defined by white mica + Na-amphibole + epidote.

Lawsonite is only locally retrogressed at rims by chlorite and quartz. Na-amphibole occurs in large subhedral crystals often replaced by chlorite + quartz + albite. Na-amphibole has a Fe-glaucophane composition (Fig. 5f). White mica occurs in different microstructural sites: syn-D₁ phengite has the highest Si content (up to 3.66 a.p.f.u.), whereas syn-D₂ phengite has Si content ranging between 3.50 and 3.38 a.p.f.u. (Fig. 5b). Syn-D₃ μm-sized crystals of epidote partially replace lawsonite, together with quartz.

Epidote + Na-amphibole + quartz veins are observed at variable angle with respect to the S₂ foliation.

Calcschists

Calcschists consist of calcite + quartz + white mica + lawsonite + chlorite + graphite and accessory phases (i.e., tourmaline, pyrite, titanite). The main foliation S₂ is defined by white mica + quartz + carbonate ± chlorite. Lawsonite occurs as large euhedral to subhedral pre-kinematic porphyroblasts. They locally include an internal schistosity (S₁), discordant with respect to the external S₂ and defined by white mica + quartz + pyrite ± graphite (Figs. 3f and 4f). Lawsonite porphyroblasts are weakly zoned; the zoning is marked by Ti- and Fe enrichments in the core, which is also characterized by higher amounts of inclusions (apatite + pyrite + quartz; Fig. 4f). Lawsonite crystals are only locally retrogressed by fine-grained quartz + white mica + calcite ± chlorite assemblages growing at rims. Three types of white mica have been recognized: phengite, muscovite, and paragonite. The three micas occur in several generations and microstructural positions. Syn-D₁ phengite (Si up to 3.63 a.p.f.u.) mainly occurs as relicts inside large lawsonite porphyroblasts along with a first generation of paragonite, generally at a high angle with respect to the main foliation. The S₂ foliation is defined by a second generation of phengite (Si from 3.35 to 3.50 a.p.f.u.) and of paragonite, while muscovite (Si < 3.30 a.p.f.u.) replaces lawsonite crystals at rims and defines an incipient syn-D₃ crenulation cleavage, at a high angle with respect of S₂ schistosity (Fig. 5b). Chlorite occurs both dispersed in the rock and along lawsonite rims.

PETROGRAPHY OF SAMPLES SELECTED FOR THE P-T MODELING

Based on their textural features and mineral assemblages, two samples (i.e., 5482: Mg-Al metagabbro; 5681: plagiogranite metabreccia, see Fig. 2c) have been selected from the main metamafic body for further petrological investigations, aimed at constraining the HP tectono-metamorphic evolution of the Albergian Unit in the upper Chisone Valley. Their petrographic features and mineral chemistry data are briefly summarized here. Modal proportions (vol.%) of the main minerals have been estimated using high-resolution multispectral maps processed using the MultiSpec© software (Fig. 6a-b). The anhydrous bulk rock compositions used for the phase diagram modeling are reported in Table 3, together with the calculated normative minerals. The blastesis-deformation relationships of the selected samples are summarized in Table 4.

Sample 5482: Mg-Al metagabbro

Sample 5482 is a fine-grained Mg-Al metagabbro characterized by a banded structure at the micro-scale (Fig. 6a). It consists of white mica (10%), albite (18%), amphibole (16%), clinopyroxene (19%), lawsonite (10.5%), garnet (1%), quartz (8%), epidote (4%), chlorite (11%), titanite (2.5%). Two types of layers can be distinguished (not thicker than 1 mm), likely deriving from mafic vs. sialic-rich levels in the gabbroic protolith. The mafic layers now consist of clinopyroxene + actinolite + chlorite + albite + titanite ± epidote, whereas the sialic layers consist of white mica + actinolite + epidote + chlorite + lawsonite + garnet (Fig. 6a). Representative analyses of mineral composition for this sample are reported in Table 1. Garnet occurs in crystals from 100 to 200 μm in size and has an almandine - spessartine-rich composition (Alm₂₈₋₅₂Sps₁₄₋₃₈Prp_{1.5-4}Grs₂₂₋₃₄). It is partially retrogressed by epidote and chlorite + white mica pseudomorphs (Fig. 6c). Lawsonite is partially retrogressed by muscovite and epidote (Fig. 6d). Relicts of Ca-clinopyroxene (from 300 to 500 μm) are still preserved in the mafic layer, within an actinolite, albite, and chlorite matrix. The “magmatic” Ca-clinopyroxene has an aegitic composition, but it contains relatively high amounts of Na (X_{Na} up to 0.20), thus suggesting that it was chemically re-equilibrated during Alpine metamorphism; it is partially replaced by omphacite and actinolite at rims. Epidote is partially retrogressed by actinolite and Mg-chlorite.

Sample 5681: Plagiogranite metabreccia

Sample 5681 metabreccia is made of plagiogranitic clasts within a mafic matrix (Fig. 6b). Clasts consist of jadeite (47%), lawsonite (23%), albite (19%), epidote (2.5%), white mica (1%), quartz (1.5%), Na-amphiboles (1%), chlorite (0.5%), rutile (1.5%) and titanite (3%). Representative analyses of mineral composition for this sample are reported in Table 2. Clasts, from mm to cm in size, are weakly foliated. Jadeite crystals, up to 500 μm in size, are set in a matrix consisting of poikiloblastic albite, quartz, and lawsonite (Fig. 6f). Jadeite is locally overgrown by Na-amphiboles, while lawsonite is retrogressed by syn-D₂ zoisite + quartz and/or syn-D₃ muscovite + epidote assemblages. The mafic matrix is made of albite (27%), Na-amphiboles (26.5%), white mica (14.5%), epidote (13%), quartz (4%), chlorite (7%), lawsonite (2.5%), rutile (2%) and titanite (3.5%). It is mainly made of the assemblage phengite + Na-amphiboles, partially retrogressed by albite + chlorite. Lawsonite occurs in lower amounts and is extensively retrogressed by the muscovite + epidote assemblage.

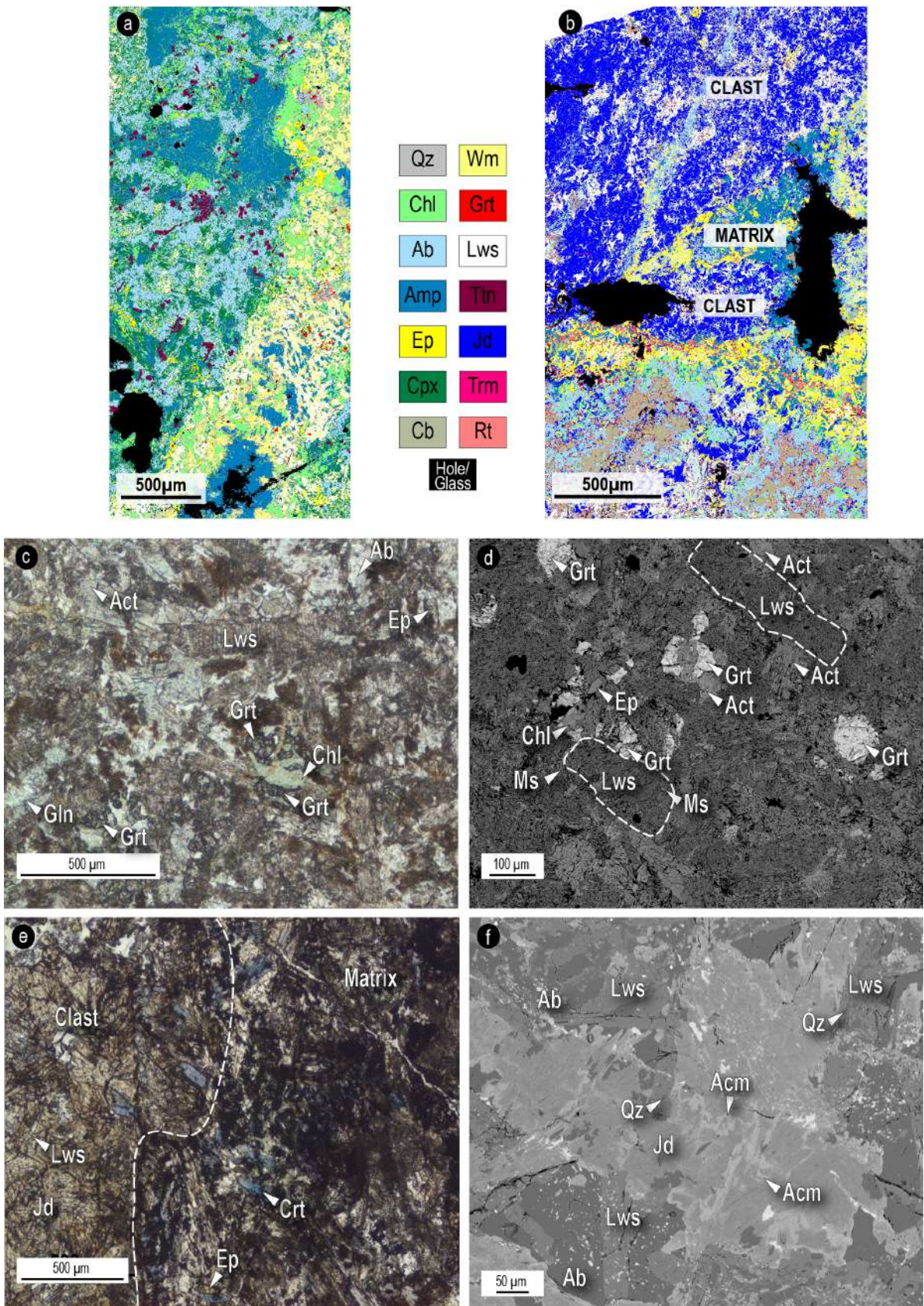


Fig. 6 - X-ray maps and representative microstructures for samples used for thermodynamic modeling. a- X-ray map of the Mg-Al metagabbro, sample 5482. b- X-ray map of the plagiogranite meta-breccia, sample 5681, with well recognizable clast and matrix relationships. c- Anhedra garnet crystals, partially retrogressed by chlorite and epidote, in sample 5482 (PPL). d- BSE detail of the silicic domain in sample 5482, showing small garnet crystals replaced by epidote and chlorite. Lawsonite is fresh and only locally replaced at rims by muscovite. e- Clast-matrix boundary in the plagiogranite metabreccia. The clast (on the left) is characterized by the widespread occurrence of jadeite crystals, lawsonite, and minor Fe-glaucophane, this last decreasing in amount away from the boundary zone. The matrix has a more retrogressed paragenesis, with a widespread occurrence of epidote-group minerals and crossite (PPL). f- BSE detail of a jadeite crystal from the plagiogranitic clast in sample 5681. Note rims and edges of acmitic composition, with albite growing both on jadeite + acmite and on lawsonite.

Table 3 - Bulk rock compositions of the two samples (5482 and 5681) used for thermodynamic modeling, calculated by combining the mineral proportions obtained from the quantitative modal estimate of SEM-EDS multispectral maps, with single-point analyses. Lower part: normative minerals calculated for these bulk-compositions.

Oxide (wt%)	SiO ₂	Al ₂ O ₃	FeO	Fe ₂ O ₃	MgO	MnO	CaO	Na ₂ O	K ₂ O	TiO ₂	Total		
5482	59.41	8.76	5.2	---	11.98	0.14	10.03	2.96	0.66	0.86	100		
5681 clasts	61.81	12.19	0.2	3.97	0.86	---	7.67	10.3	0.08	2.92	100		
5681 matrix	59.22	12.2	4.43	---	7.59	---	6.35	5.42	1	3.8	100		
Normative minerals	Quartz	Pl	Or	Di	Hy	Wo	Acm	Ilm	Hem	Ttn	Mag	Ap	Na ₂ SiO ₃ *
5482	6.05	33.59	3.9	30.95	22.82	---	---	1.63	---	---	0.29	---	---
5681 clasts	2.29	63.85	0.47	1.88	---	8.76	8.54	0.42	---	6.6	---	0.76	2.76
5681 matrix	3.59	51.87	5.91	20.05	11.36	---	---	7.22	---	---	---	---	---

*= sodium metasilicate

Table 4 - Blastesis-deformation relationships for the two rock samples used for thermodynamic modeling (samples 5482 and 5681).

	5482			5681		
	D1	D2	D3	D1	D2	D3
Grt	—	—	—	—	—	—
Cpx	Ang — Omp	—	—	Jd — Acm	—	—
Lws	—	—	—	—	—	—
Wm	Ph	Ph	Ms	Ph	Ph	Ms
Amp	Gln/Act	Grt/Act	Act	Gln	Grt	—
Qz	—	—	—	—	—	—
Ep	—	Zo — Ep	—	—	Zo — Ep	—
Chl	—	—	—	—	—	—
Ab	—	—	—	—	—	—
Ttn	—	—	—	—	—	—
Rt	—	—	—	—	—	—

THERMODYNAMIC MODELING

The peak P-T conditions of the selected samples were constrained using the isochemical phase diagram approach, based on the predicted stability field of the observed assemblages, combined with the intersection of compositional isopleths modeled for white mica and clinopyroxene (for both samples), and for garnet (for sample 5482). P-T isochemical phase diagrams were calculated for a garnet + omphacite Mg-Al metagabbro (sample 5482) and a plagiogranitic metabreccia (sample 5681). For this second sample, two distinct phase diagrams have been calculated, one for the plagiogranitic clasts, and one for the mafic matrix, due to the significant difference in mineral assemblages and bulk compositions

between the two domains. Bulk rock compositions of these samples (Table 3) were calculated by combining the mineral proportions obtained from the quantitative modal estimate of SEM-EDS multispectral maps, with single-point analyses. For these bulk-compositions, normative minerals have been also calculated (Table 3).

The coarse-grained relicts of “magmatic” clinopyroxenes have not been fractionated in the calculation of the bulk composition of sample 5482, because they were involved in the Alpine metamorphic re-equilibration, as witnessed by their relatively high Na contents.

The P-T pseudosection for sample 5482 was calculated in the system MnNCFMASTH (MnO-Na₂O-CaO-FeO-MgO-Al₂O₃-SiO₂-TiO₂-H₂O). For sample 5681, the P-T pseudosection

of the plagiogranitic clasts was calculated in the system NCKFMASHTO (Na₂O-CaO-K₂O-FeO-MgO-Al₂O₃-SiO₂-TiO₂-O₂-H₂O), while that for the mafic matrix was calculated in the system NCKFMASHT (Na₂O-CaO-K₂O-FeO-MgO-Al₂O₃-SiO₂-TiO₂-H₂O). All the isochemical phase diagrams were calculated using *Perple_X* 6.9.0 (Connolly, 1990; 2005; 2009), the internally consistent thermodynamic database of Holland and Powell (2011) (*ds62*), and the equation of state for H₂O of Holland and Powell (1998). Fluid saturated conditions were assumed, and the fluid was considered as pure H₂O ($a_{\text{H}_2\text{O}} = 1$). This last assumption is realistic for the studied samples, because of the large occurrence of hydrous phases and the absence of primary carbonates and sulfides.

MnO was neglected in the pseudosection calculated for sample 5681 (both for clasts and matrix) because Mn-bearing phases are lacking. Fe³⁺ was neglected in pseudosections of samples 5482 and the matrix of sample 5681, because Fe³⁺-rich oxides are absent and the amount of Fe³⁺ in the analyzed minerals is very low. On the opposite, Fe³⁺ was considered for the clasts of sample 5681, due to the occurrence of aegirine-rich clinopyroxenes. The following solid solution models were used: biotite, chlorite, garnet, white mica (White et al., 2014), clinopyroxene (Green et al., 2007), amphibole (Green et al., 2016), feldspar (Fuhrman and Lindsley, 1988), and epidote (Holland and Powell, 1998). Quartz, lawsonite, talc, and kyanite were considered as pure phases.

In all the calculated phase diagrams, lawsonite is predicted to be stable at lower T and high-P conditions with respect to epidote; the lawsonite-to-epidote transition is marked by a (nearly) discontinuous reaction with a positive slope, ranging from about 450°C, 14 kbar to 550°C, 20 kbar. White mica and quartz are predicted to be stable in almost the whole P-T region of interest in sample 5482; jadeite and quartz are modeled in all the fields of the pseudosection calculated for the plagiogranitic clasts of sample 5681, whereas white mica, Na-amphibole, jadeite, and quartz are predicted to be stable in all the fields of the pseudosection calculated for the matrix of sample 5681.

Sample 5482

The modeled isochemical phase diagram is dominated by large trivariant fields and minor di- and four-variant fields (Fig. 7a). The diagram is crossed by a thin but extended divariant field marking the miscibility gap between two types of clinopyroxenes: Cpx1 is a Ca- and Mg-rich clinopyroxene, with low X_{Na} values ($X_{\text{Na}} = \text{Na}/(\text{Na} + \text{Ca})$) and it is predicted to be stable at lower-T and higher-P conditions, whereas Cpx2 is an omphacite (Ca-Na clinopyroxene) and it is predicted to occur at higher-T and lower-P conditions. In this sample, the microstructural relicts of the coarse-grained magmatic clinopyroxene are mostly Ca-rich clinopyroxenes containing low amounts of Na ($X_{\text{Na}} = 0.09-0.20$), whereas omphacitic compositions are observed for the fine-grained clinopyroxenes in the matrix. The microstructural relicts of “magmatic” clinopyroxene do not preserve their original composition, but they were instead re-equilibrated during the HP metamorphic peak. Although not commonly reported, a similar change in composition from Ca-rich clinopyroxenes with low X_{Na} content, to Ca-Na clinopyroxenes (i.e., omphacite, with $X_{\text{Na}} > 0.20$), has been observed in other low-grade lawsonite blueschist-facies units, including Alpine Corsica (Piccoli et al., 2018) and Chugoku mountains of south-western Japan (Tsujimori and Liou, 2007). These clinopyroxenes have not been fractionated in the calculation of the bulk rock, because their compositions changed during Alpine metamor-

phism, as witnessed by Na content. On the other hand, the fine-grained omphacite in the matrix grew during a first stage of moderate heating and decompression related to the first tectono-metamorphic event (D₁, see Table 4).

The observed peak assemblage (Na-amphibole + Ca-amphibole + Grt + Cpx1 + Lws + Qz + Wm + Ttn) is modeled by a large tri-variant field at T < 480°C and P = 16-22 kbar; this field is bounded by the appearance of Cpx2 at higher temperatures (T > 470°C), and by the appearance of zoisite and talc at lower (P < 16 kbar) and higher (P > 22 kbar) pressures, respectively. It is also worth noticing that titanite is the Ti-rich mineral predicted to be stable in this field, in agreement with the petrographic observations. The modeled garnet (Alm₂₈₋₅₂Sps₁₄₋₃₈Prp_{1.5-4}Grs₂₂₋₃₄) and clinopyroxene (Cpx1: X_{Na} = 0.09-0.20) compositional isopleths allow to further constrain the peak P-T conditions of this sample at 21±1.5 kbar and 450±30°C.

Sample 5681

The pseudosection modeled for the matrix of this sample is characterized by large tri-variant fields and minor narrow di-variant fields (Fig. 7b). The observed peak assemblage (Qz + Jd + Wm + Na-amp + Lws + Ttn + Rt) is predicted by a tri-variant field at T < 450°C, limited toward lower pressures by the appearance of paragonitic mica, and toward higher pressures by the appearance of an omphacitic clinopyroxene. The modeled compositional isopleths of jadeite corresponding to its measured composition in the matrix ($X_{\text{Na}} = 0.87-0.94$) are consistent with the predicted mineral assemblage. The modeled compositional isopleths for syn-D₁ phengite flakes (Si = 3.67 - 3.40 a.p.f.u.) allow to better constrain the P-T conditions at 18 ± 2 kbar and 410±20°C.

The phase diagram modeled for the plagiogranitic clast is characterized by large quadri-variant fields and minor narrow tri-variant fields (Fig. 7c). The observed mineral assemblage (Jd + Qz + Wm + Lws + Ttn + Rt) encompasses a large quadri-variant field. It is worth noticing that, in agreement with the petrographic observations, titanite is predicted to occur in the modeled assemblage. A tighter constrain of the P-T conditions is possible thanks to modeled compositional isopleths for jadeite (X_{Na}) and white mica (Si a.p.f.u.). The measured Si values for the syn-D₁ phengite flakes (Si = 3.40-3.67 a.p.f.u.) better constrain temperatures at T < 450°C. At the same time, the lowest X_{Na} values of modeled isopleths for peak-related jadeite ($X_{\text{Na}} = 0.87$) fit well in the range of T < 430°C and P of 21-24 kbar. The intersection of the estimated P-T conditions for matrix and clasts plots in a relatively small field at 400±20°C and 19±1 kbar.

DISCUSSION

New P-T estimates for the Albergian Unit

The isochemical phase diagram approach allowed to constrain the Alpine peak metamorphic conditions experienced by the Albergian Unit and to qualitatively infer its exhumation history (Fig. 7d). The D₁ tectono-metamorphic event, occurred at the metamorphic peak, is constrained at 19±1 kbar and 400±20°C in the lawsonite stability field, where the ellipses show the constrained P-T conditions, based on the mineral assemblages and the intersection of compositional isopleths, as indicated in each legend (Fig. 7a-c). For this area, Agard et al. (2001) and Beyssac et al. (2002) predicted P-T conditions of 18-21 kbar and 380-430°C, estimated

chlorite + paragonite ± potassium white mica and/or zoisite + Na-amphibole overgrow lawsonite crystals (Fornieris and Holloway, 2003), documenting lawsonite breakdown in the epidote blueschist-facies. As reported by Shelley and Bossiere (1999) these types of lawsonite retrogression do not imply the release of significant amounts of water, hence no widespread retrogression occurred and Na-amphibole + epidote assemblages are still well preserved in the main S_2 foliation. A geothermal gradient of about 10-12°C/km can be inferred for the development of this schistosity, at 11-13 kbar and 450-500°C, well within the glaucophane + paragonite stability field (see Fig. 7d). Widespread retrogression occurring in the D_3 event developed at $P < 5$ kbar and $T < 350^\circ\text{C}$ along a 25°C/km geothermal gradient, as suggested by the occurrence of the later albite + chlorite + quartz assemblage.

The P-T path reconstructed describes a clockwise trajectory, from the D_2 event consistent with other trajectories recently constrained with similar methods in adjacent areas (Ghignone et al., 2020; Corno et al., 2021). Furthermore, the estimated peak P-T conditions and the preservation of abundant fresh lawsonite imply that the Albergian Unit experienced a cold subduction (Martin et al., 2014).

Widespread lawsonite occurrence in the AU metamafic rocks

The HP/LT to LP/LT Alpine tectono-metamorphic evolution was responsible for intense transpositions and overprinting of folding in the AU (such as in its adjacent units, e.g., Caron, 1977; Malusà et al., 2002). The highly competent metamafic bodies embedded in the calcschists were low-strain domains which preserved pre-metamorphic and peak metamorphic assemblages. Abundant lawsonite has been preserved in those lithologies, such as metagabbros, where the original magmatic texture is still conserved.

In these metamafic rocks (where deformation is not enhanced by pervasive fluid circulation as in the embedding calcschists), equilibrium conditions were not achieved during retrogression: this allowed the preservation of metastable phases such as lawsonite, even though the exhumation trajectory of AU (Fig. 7d) plots in the stability field of epidote. Thus, the metamafic rocks are considerably more useful than calcschists in unraveling the peak metamorphic history of AU (i.e., a segment of the Liguria-Piemonte ocean).

Usually, the development of lawsonite in cold subduction zones has been linked to fluids coming from the downgoing slab (see Tsujimori and Ernst, 2014, for a review). Specifically, the abundance of lawsonite in calcschists has been explained in the blueschist-facies of the Western Alps through mass transfer of H_2O and decarbonation processes (Vitale Brovarone et al., 2014a; Lefeuvre et al., 2020). These fluid-rock interaction processes, testified by abundant lawsonite crystallization in HP/LT veins as well as in metasomatic rocks, has been observed worldwide from the Alpine Corsica (Vitale Brovarone, 2014b; Piccoli et al., 2018) to the Zagros orogen in southeastern Iran (Munoz-Montecinos et al., 2021). However, bulk rock composition is of primary importance to explain lawsonite crystallization in metamafic rocks (Wei and Clark, 2011; Tsujimori and Ernst, 2014). The normative minerals predicted from the measured bulk rock compositions are in agreement with the assumed protoliths' nature (see Table 3), thus suggesting that the systems remained closed during the whole metamorphic evolution. Hence, the widespread crystallization of lawsonite in metamafic rocks can be related to the breakdown of magmatic Ca-rich plagioclase and its hydration (anorthite *sensu*

lato) and/or to the large carbon content, as noticed also by other authors (Pognante, 1989; Martin et al., 2014, for a review). To preserve metastable lawsonite in such amounts, Clarke et al. (2006) envisaged a cold geothermal gradient and exhumation processes accompanied by substantial cooling. However, an alternative exhumation process can be inferred to justify the incomplete retrogression of lawsonite in the epidote stability field. Wei and Clark (2011) in fact suggested the occurrence of an exhumation sufficiently fast for lawsonite to be preserved in favorable structural and textural domains.

CONCLUSIONS

- The Albergian Unit includes segments of oceanic crust made of gabbro apophysis and related volcanic and volcano-sedimentary cover, now embedded in carbonate-rich metasediments.
- Lawsonite is preserved in metamafic rocks as well as in metasediments. Since major veins, witnessing mass transfer of fluids, developed after the D_2 event and lawsonite is linked to the prograde metamorphic stages (D_1 event), the observed lawsonite in the AU did not grow in relation to decarbonation processes and mass transfer of fluids but might be connected to favorable Ca-rich bulk compositions. The weak D_3 retrogressive event permitted widespread preservation of fresh metastable lawsonite.
- The abundance of metastable lawsonite in the AU, and its minor occurrence in the surrounding units, could be linked to fast exhumation processes rather than different tectonic conditions (as suggested by Zack et al., 2004). In fact, fast exhumation hampered lawsonite-epidote substitution and favoured the preservation of a large amount of metastable lawsonite.
- Due their different rheologies and responses to strain, metasedimentary lithologies and oceanic metamafic rocks may record differently the Alpine metamorphic peak. Hence, metamorphic assemblages preserved by rock successions with bulk compositions less prone to a good conservation of peak mineral assemblages, could lead to a misunderstanding of the true peak P-T conditions.

ACKNOWLEDGMENTS

We wish to thank the two anonymous Reviewers for their constructive comments on the first draft of this manuscript. We are thankful to J.A. Padrón Navarta for his editorial job, which further improved the last draft of this work. A.C. is grateful to M. Giovo for the landscape picture of Fig. 1. This research was funded by research Grants from University of Torino, Ricerca Locale “ex 60%” (A.B., A.C. and M.G.).

REFERENCES

- Agard P., 2021. Subduction of oceanic lithosphere in the Alps: Selective and archetypal from (slow-spreading) oceans. *Earth Sci. Rev.*, 103517.
- Agard P., Vidal O. and Goffé B., 2001. Interlayer and Si content of phengite in HP-LT carpholite-bearing metapelites. *J. Metam. Geol.*, 19 (5): 479-495.
- Beyssac O., Rouzaud JN., Goffé B., Brunet F. and Chopin C., 2002. Graphitization in a high-pressure, low-temperature metamorphic gradient: a Raman microspectroscopy and HRTEM study. *Contrib Mineral Petrol*, 143, 19-31.

- Beltrando M., Compagnoni R. and Lombardo B., 2010. (Ultra-) High-pressure metamorphism and orogenesis: An Alpine perspective. *Gondwana Res.*, 18: 147-166.
- Burroni A., Levi N., Marroni M. and Pandolfi L., 2003. Lithostratigraphy and structure of the Lago Nero Unit (Chenaillet Massif, Western Alps): comparison with Internal Liguride units of Northern Apennines. *Ophioliti*, 28 (1): 1-11.
- Caron J.M., 1974. Rapports entre diverses "générations" de lawsonite et les déformations dans les Schistes lustrés des Alpes cottiennes septentrionales (France et Italie). *Bull. Soc. Géol. Fr.*, 7 (3): 255-263.
- Caron J.M., 1977. Lithostratigraphie et tectonique des Schistes lustrés dans les Alpes cottiennes septentrionales et en Corse orientale. PhD Thesis, Université de Strasbourg, 170 pp. <https://tel.archives-ouvertes.fr/tel-00805504>.
- Clarke G.L., Powell R. and Fitzherbert J.A., 2006. The lawsonite paradox: a comparison of field evidence and mineral equilibria modelling. *J. Metam. Geol.*, 24: 715-725.
- Compagnoni R., 1977. The Sesia-Lanzo Zone: High pressure-low temperature metamorphism in the Austroalpine continental margin. *Rend. Soc. It. Miner. Petrol.*, 33 (1): 335-374.
- Connolly J.A.D., 1990. Multivariable phase diagrams: An algorithm based on generalized thermodynamics. *Am. J. Sci.*, 290: 666-718.
- Connolly J.A.D., 2005. Computation of phase equilibria by linear programming: A tool for geodynamic modeling and its application to subduction zone decarbonation. *Earth Planet. Sci. Lett.*, 236 (1-2): 524-541.
- Connolly J.A.D., 2009. The geodynamic equation of state: What and how. *Geochem., Geophys. Geosyst.*, 10 (10): 1-19.
- Corno A., Groppo C., Mosca P., Borghi A. and Gattiglio M., 2021. Eclogitic metamorphism in the Alpine far-west: petrological constraints on the Banchetta-Rognosa tectonic unit. *Swiss J. Geosci.* 114: 16.
- Corno A., Mosca P., Borghi A. and Gattiglio M., 2019. Lithostratigraphy and petrography of the Monte Banchetta-Punta Rognosa oceanic succession (Tronca and Chisonetto Valleys, Western Alps). *Ophioliti*, 44 (2): 83-95.
- Cook-Kollars J., Bebout G.E., Collins N.C., Angiboust S. and Agard P., 2014. Subduction zone metamorphic pathway for deep carbon cycling: I. Evidence from HP/UHP metasedimentary rocks, Italian Alps. *Chem. Geol.*, 386: 31-48.
- Desmons J., 1990. Sur quelques minéraux de la zone piémontaise (Zone du Combin) dans les Alpes françaises. *Géol. Alp.*, 66 : 23-38.
- Ellenberger F., 1960. Sur une paragenèse éphémère à lawsonite et glaucophane dans le métamorphisme alpin en Haute-Maurienne (Savoie). *Bull. Soc. Geol. Fr.*, 7 (2): 190-194.
- Faccenda M., 2014. Water in the slab: A trilogy. *Tectonophysics*, 614: 1-30.
- Forneris J.F. and Holloway J.R., 2003. Phase equilibria in subducting basaltic crust: implications for H₂O release from the slab. *Earth Planet. Sci. Lett.* 214 (1-2): 187-201.
- Franchi S., 1895. Alcune metamorfosi di eufotidi e diabasi Alpi Occid. *Boll. R. Com. Geol. d'It.*, 181.
- Franchi S., 1897. Sopra alcuni nuovi giacimenti di rocce a lawsonite. *Boll. Soc. Geol. It.*, 16: 73-76.
- Fuhrman M.L. and Lindsley D.H., 1988. Ternary-Feldspar modeling and thermometry. *Am. Miner.*, 73 (3-4): 201-215.
- Ghignone S., Borghi A., Balestro G., Castelli D., Gattiglio M. and Groppo C., 2020. HP tectono-metamorphic evolution of the Internal Piedmont Zone in Susa Valley (Western Alps): New petrologic insight from garnet + chloritoid-bearing micaschists and Fe-Ti metagabbro. *J. Metam. Geol.* 39 (4): 391-518.
- Goto A., Kunugiza K. and Omori S., 2007. Evolving fluid composition during prograde metamorphism in subduction zones: A new approach using carbonate-bearing assemblages in the pelitic system. *Gondw. Res.*, 11 (1-2): 166-179.
- Green E., Holland T. and Powell R., 2007. An order-disorder model for omphacitic pyroxenes in the system jadeite-diopside-hedenbergite-acmite, with applications to eclogitic rocks. *Am. Miner.*, 92 (7): 1181-1189.
- Green E.C.R., White R.W., Diener J.F.A., Powell R., Holland T.J.B. and Palin R.M., 2016. Activity-composition relations for the calculation of partial melting equilibria in metabasic rocks. *J. Metam. Geol.*, 34 (9): 845-869.
- Groppo C. and Castelli D., 2010. Prograde P-T evolution of a lawsonite eclogite from the Monviso meta-ophiolite (Western Alps): dehydration and redox reactions during subduction of oceanic FeTi-oxide gabbro. *J. Petrol.*, 51 (12): 2489-2514.
- Hawthorne F.C., Oberti R., Harlow G.E., Maresch W.V., Martin R.F., Schumacher J.C. and Welch M.D., 2012. Nomenclature of the amphibole supergroup. *Am. Miner.*, 97 (11-12): 2031-2048.
- Holland T.J.B. and Powell R., 1998. An internally consistent thermodynamic dataset for phases of petrological interest. *J. Metam. Geol.*, 16: 309-343.
- Holland T.J.B. and Powell R., 2011. An improved and extended internally consistent thermodynamic dataset for phases of petrological interest, involving a new equation of state for solids. *J. Metam. Geol.*, 29: 333-383.
- Lefevre B., Agard P., Verlaquet A., Dubacq B. and Plunder A., 2020. Massive formation of lawsonite in subducted sediments from the Schistes Lustrés (W. Alps): Implications for mass transfer and decarbonation in cold subduction zones. *Lithos*, 370: 105629.
- Malusà M.G., Mosca P., Borghi A., Dela Pierre F. and Polino R., 2002. Approccio multidisciplinare per la ricostruzione dell'assetto tettono-stratigrafico e dell'evoluzione metamorfica-strutturale di un settore di catena orogenica: l'esempio dell'Alta Valle di Susa (Alpi Occidentali). *Boll. Soc. Geol. It.*, 57: 249-257.
- Martin S. and Tartarotti P., 1989. Polyphase HP metamorphism in the ophiolitic glaucophanites of the lower St. Marcel valley (Aosta Valley).
- Martin L.A.J., Hermann J., Gauthiez-Putallaz L., Whitney D.L., Vitale Brovarone A., Fornash K.F. and Evans N.J., 2014. Lawsonite geochemistry and stability-implication for trace element and water cycles in subduction zones. *J. Metam. Geol.*, 32 (5): 455-478.
- Mével C. and Kienast J.R., 1980. Chromian jadeite, phengite, pumpellyite, and lawsonite in a high-pressure metamorphosed gabbro from the French Alps. *Miner. Mag.*, 43 (332): 979-984.
- Morimoto N., 1988. Nomenclature of pyroxenes. *Schw. Miner. Petrogr. Mitt.*, 68: 95-111.
- Muñoz-Montecinos J., Angiboust S., Garcia-Casco A., Glodny J. and Bebout G., 2021. Episodic hydrofracturing and large-scale flushing along deep subduction interfaces: Implications for fluid transfer and carbon recycling (Zagros Orogen, southeastern Iran). *Chem. Geol.*, 571: 120173.
- Nitsch K.H., 1972. Das P-T-X_{CO2} Stabilitätsfeld von Lawsonit. *Contrib. Miner. Petrol.* 34: 116-134.
- Petrakakis K., and Dietrich H., 1985. MINSORT: A program for the processing and archivation of microprobe analysis of silicate and oxide minerals. *N. Jahrb. Miner. Abhandl.*, 8: 379-384.
- Piana F., Fioraso G., Irace A., Mosca P., D'atri A., Barale A., Falletti P., Monegato G., Morelli M., Tallone S. and Vigna G.B., 2017. Geology of Piemonte region (NW Italy, Alps-Apennines interference zone). *J. Maps*, 13 (2): 395-405.
- Piccoli F., Brovarone A.V. and Ague J.J., 2018. Field and petrological study of metasomatism and high-pressure carbonation from lawsonite eclogite-facies terrains, Alpine Corsica. *Lithos*, 304: 16-37.
- Pognante U., 1989. Lawsonite, blueschist and eclogite formation in the Southern Sesia Zone (Western Alps, Italy). *Eur. J. Miner.*, 1, 89-104.
- Pognante U., 1991. Petrological constraints on the eclogite- and blueschist-facies metamorphism and P-T-t paths in the western Alps. *Journal of Metamorphic Geology*, 9(1): 5-17.
- Pognante U., Compagnoni R. and Gosso G., 1980. Micro-meso-structural relationships in the continental eclogitic rocks of the Sesia-Lanzo Zone (Italian Western Alps): a record of subduction cycle. *Rend. Soc. It. Miner. Petrol.*, 36 (1): 169-186.
- Poli S. and Schmidt M.W., 1998. The high-pressure stability of zoisite and phase relationships of zoisite-bearing assemblages. *Contrib. Miner. Petrol.*, 130 (2): 162-175.

- Poli S., Franzolin E., Fumagalli P. and Crottini A., 2009. The transport of carbon and hydrogen in subducted oceanic crust: An experimental study to 5 GPa. *Earth Planet. Sci. Lett.*, 278 (3-4): 350-360.
- Polino R. and Lemoine M., 1984. Détritisme mixte d'origine continentale et océanique dans les sédiments jurassico-crétacés supra-ophiolitiques de la Téthys ligure: la série du Lago Nero (Alpes Occidentales franco-italiennes). *C.R. séances Acad. Sci. Série 2*, 298: 359-364.
- Polino R., Borghi A., Carraro F., Dela Pierre F., Fioraso G. and Giardino M., 2002. Note illustrative della Carta Geologica d'Italia alla scala 1: 50.000, F. 132-152-153 "Bardonecchia". Regione Piemonte, Direz. Region. Servizi Tecn. Prevenz.. Litografia Geda, Nichelino. Torino.
- Polino R., Monticelli F. and Vaccaro D., 1983. L'unità piemontese Chaberton-Grand Hoche (Val Susa-Alpi Occidentali): evoluzione litostratigrafica, assetto strutturale e rapporti con i complessi circostanti. *Mem. Soc. Geol. It.*, 26 (2): 489-498.
- Scarsi M., Malatesta C. and Fornasaro S., 2018. Lawsonite-bearing eclogite from a tectonic mélange in the Ligurian Alps: new constraints for the subduction plate-interface evolution. *Geol. Mag.*, 155 (2): 280-297.
- Schmidt M.W. and Poli S., 1994. The stability of lawsonite and zoisite at high pressures: Experiments in CASH to 92 kbar and implications for the presence of hydrous phases in subducted lithosphere. *Earth Planet. Sci. Lett.*, 124 (1-4): 105-118.
- Servizio Geologico d'Italia, 2002. Carta Geologica d'Italia alla scala 1:50.0000, F. 154 Susa, Regione Piemonte, Direz. Region. Servizi Tecn. Prevenz.. Litografia Geda, Nichelino. Torino.
- Servizio Geologico d'Italia, 2002. Carta Geologica d'Italia alla scala 1:50.0000, F. 132-152-153 Bardonecchia Regione Piemonte, Direz. Region. Servizi Tecn. Prevenz. Litografia Geda, Nichelino. Torino.
- Servizio Geologico d'Italia, 2020. Carta Geologica d'Italia alla scala 1:50.0000, F. 171 Cesana. http://www.isprambiente.gov.it/Media/carg/171_CESANA_TORINESE/Foglio.html
- Shelley D. and Bossière G., 1999. Ile de Groix: retrogression and structural developments in an extensional régime. *J. Struct. Geol.*, 21 (10): 1441-1455.
- Tsujimori T. and Ernst W.G., 2014. Lawsonite blueschists and lawsonite eclogites as proxies for palaeo-subduction zone processes: a review. *J. Metam. Geol.*, 32 (5): 437-454.
- Tsujimori T. and Liou J. G., 2007. Significance of the Ca-Na pyroxene-lawsonite-chlorite assemblage in blueschist-facies metabasalts: An example from the Renge metamorphic rocks, southwest Japan. *Intern. Geol. Rev.*, 49 (5): 416-430.
- van Keken P.E., Hacker B.R., Syracuse E.M. and Abers G.A., 2011. Subduction factory: 4. Depth-dependent flux of H₂O from subducting slabs worldwide. *J. Geophys. Res., Solid Earth*, 116 (B1).
- Vitale Brovarone A., Beyssac O., Malavieille J., Molli G., Beltrando M. and Compagnoni R., 2013. Stacking and metamorphism of continuous segments of subducted lithosphere in a high-pressure wedge: the example of Alpine Corsica (France). *Eart Sci. Rev.*, 116, 35-56.
- Vitale Brovarone A., Alard O., Beyssac O., Martin L. and Picatto M., 2014b. Lawsonite metasomatism and trace element recycling in subduction zones. *J. Metam. Geol.*, 32 (5): 489-514.
- Vitale Brovarone A., Groppo C., Hetényi G., Compagnoni R. and Malavieille J., 2011. Coexistence of lawsonite-bearing eclogite and blueschist: phase equilibria modelling of Alpine Corsica metabasalts and petrological evolution of subducting slabs. *J. Metam. Geol.*, 29 (5): 583-600.
- Vitale Brovarone A., Picatto M., Beyssac O., Lagabrielle Y. And Castelli D., 2014a. The blueschist-eclogite transition in the Alpine chain: P-T paths and the role of slow-spreading extensional structures in the evolution of HP-LT mountain belts. *Tectonophysics*, 615, 96-121.
- Vitale Brovarone A., Tumiami S., Piccoli F., Ague J.J., Connolly J.A. and Beyssac O., 2020. Fluid-mediated selective dissolution of subducting carbonaceous material: Implications for carbon recycling and fluid fluxes at forearc depths. *Chem. Geol.*, 549, 119682.
- Wei C.J. and Clarke G.L., 2011. Calculated phase equilibria for MORB compositions: a reappraisal of the metamorphic evolution of lawsonite eclogite. *J. Metam. Geol.*, 29 (9): 939-952.
- White R.W., Powell R., Holland T.J.B., Johnson T.E. and Green E.C.R., 2014. New mineral activity-composition relations for thermodynamic calculations in metapelitic systems. *J. Metam. Geol.*, 32 (3): 261-286.
- Whitney D.L. and Evans B.W., 2010. Abbreviations for names of rock-forming minerals. *Am. Miner.*, 95 (1): 185-187.
- Whitney D. L., Fornash K.F., Kang P., Ghent E.D., Martin L., Okay A. I. and Brovarone A.V., 2020. Lawsonite composition and zoning as tracers of subduction processes: A global review. *Lithos*, 370, 105636.
- Zack T., Rivers T., Brumm R. and Kronz A., 2004. Cold subduction of oceanic crust: Implications from a lawsonite eclogite from the Dominican Republic. *Eur. J. Miner.*, 16: 909-916.
- Zucali M. and Spalla M.I., 2011. Prograde lawsonite during the flow of continental crust in the Alpine subduction: Strain vs. metamorphism partitioning, a field-analysis approach to infer tectonometamorphic evolutions (Sesia-Lanzo Zone, Western Italian Alps). *J. Struct. Geol.*, 33 (3): 381-398.

Received, February 7, 2022

Accepted, April 25, 2022

First published online, May 1, 2022